NASA CR-72367

NASA

HIGH TEMPERATURE DEFORMATION OF DISPERSION STRENGTHENED NICKEL ALLOYS

I. The Influence of Initial Structure on Tensile and Creep Deformation of TD Nickel

II. The Effect of Matrix Stacking Fault Energy on Creep of Ni-Cr-ThO$_2$ Alloys

by

B. A. Wilcox and A. H. Clauer

prepared for

NATIONAL AERONAUTICS AND SPACE ADMINISTRATION

CONTRACT NAS 3-9413

February 29, 1968

BATTELLE MEMORIAL INSTITUTE
COLUMBUS LABORATORIES

Requests for copies of this report should be referred to:

National Aeronautics and Space Administration
Scientific and Technical Information Division
Attention: USS-A
Washington, D. C. 20546

FINAL REPORT

on

HIGH TEMPERATURE DEFORMATION OF DISPERSION
STRENGTHENED NICKEL ALLOYS

I.   The Influence of Initial Structure on Tensile and
     Creep Deformation of TD Nickel

II. The Effect of Matrix Stacking Fault Energy on Creep
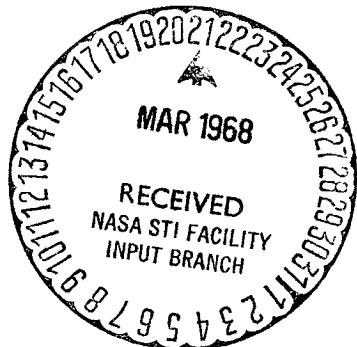   of $Ni-Cr-ThO_2$ Alloys

by

B. A. Wilcox and A. H. Clauer

prepared for

NATIONAL AERONAUTICS AND SPACE ADMINISTRATION

February 29, 1968

CONTRACT NAS 3-9413

Technical Management
NASA Lewis Research Center
Cleveland, Ohio 44135
F. H. Harf
C. W. Andrews

BATTELLE MEMORIAL INSTITUTE
Columbus Laboratories
505 King Avenue
Columbus, Ohio 43201

HIGH TEMPERATURE DEFORMATION OF DISPERSION STRENGTHENED NICKEL ALLOYS

by

B. A. Wilcox and A. H. Clauer

ABSTRACT

I. The Influence of Initial Structure on Tensile and Creep Deformation of TD Nickel

Tensile deformation studies on as-received and recrystallized TD Nickel were conducted over the temperature range 25-1200 °C. Over the entire range, the yield strength of the recrystallized material was greater than that of pure polycrystalline nickel. A further yield strength increment was observed for the as-received TD Nickel bar over the whole range of test temperatures. These results are interpreted in terms of <u>direct</u> and <u>indirect</u> strengthening by the ThO_2 particles. High temperature creep studies showed that as-received TD Nickel was considerably stronger than the recrystallized material. In neither case, however, could the results be interpreted in terms of present creep theories.

Part II. The Effect of Matrix Stacking Fault Energy on Creep of Ni-Cr-ThO₂ Alloys

High temperature creep tests on $Ni-1ThO_2$, $Ni-13.5Cr-1ThO_2$, $Ni-22.6Cr-1ThO_2$ and $Ni-33.7Cr-1ThO_2$ alloys revealed that Cr additions significantly lowered the steady-state creep rate, $\dot{\epsilon}_s$. This was attributed to Cr lowering the matrix stacking fault energy, γ, and it was found that $\dot{\epsilon}_s \propto \gamma^m$ where m = 3.1-3.3.

TABLE OF CONTENTS

LIST OF TABLES

LIST OF FIGURES

LIST OF FIGURES
(Continued)

HIGH TEMPERATURE DEFORMATION OF DISPERSION STRENGTHENED NICKEL ALLOYS

by

B. A. Wilcox and A. H. Clauer

SUMMARY

This program was conducted in two parts: I. A study to determine the influence of initial structure on the tensile (25-1200 °C) and creep (650-1100 °C) deformation of TD Nickel; and II. An investigation of the effects of stacking fault energy on the high temperature creep (700-1100 °C) of experimental Ni-Cr-ThO$_2$ alloys.

Part I. The tensile and creep characteristics of as-received TD Nickel bar were compared with those of the same material which had been cold worked 95% and recrystallized at 1300 °C. The higher yield strengths of recrystallized TD Nickel, compared with pure polycrystalline nickel, were attributed to direct strengthening by the ThO$_2$ particles. This strength increment was best rationalized in terms of the Orowan hardening mechanism. An additional increment in yield strength was observed for the as-received TD Nickel bar over the entire test temperature range. This indirect strengthening due to the ThO$_2$ particles arose because the particles promoted a stable, elongated, fine-grained structure during fabrication, i.e., a high stored energy of cold work.

The recrystallized TD Nickel was much weaker in high temperature creep than the as-received bar. Two empirical creep equations could be used to express the effects of stress and temperature on the steady-state creep rate, $\dot{\epsilon}_s$. However, it was not possible to explain the creep behavior of either as-received or recrystallized TD Nickel in terms of present creep theories.

$$\dot{\epsilon}_s = A\sigma^n \exp-\left(\frac{Q_c}{RT}\right) \quad ,$$

$$\dot{\epsilon}_s = A'e^{B\sigma} \exp-\left(\frac{Q_c}{RT}\right) \quad .$$

Creep Parameter	As-received TC Nickel bar (From Ref. 1)	Recrystallized TD Nickel
Q_c	190 kcal/mole	235 kcal/mole
n	40, over σ range 15-20 ksi	119, high stresses 15, low stresses
B	2.3 x 10^{-3} psi^{-1}, over σ range 15-20 ksi	5.4 x 10^{-3} psi^{-1}, high stresses 1.5 x 10^{-3} psi^{-1}, low stresses

Part II. Additions of up to approximately 30 wt % Cr to a Ni-1ThO$_2$ base alloy lowered the steady-state creep rate in the same manner as do Cr additions to pure poly-crystalline Ni. For example, at a given stress and temperature the creep rate of Ni-33.7Cr-1ThO$_2$ was ~300 times lower than that of Ni-1ThO$_2$. The lower creep rate in Cr-containing alloys was attributed to the fact that Cr lowers the stacking fault energy of the matrix. It is probable that the rate-controlling creep process was self-diffusion controlled, and the results were interpreted by the creep formulation of Sherby and co-workers[2,3].

$$\dot{\epsilon}_s = C\, \gamma^m\, (\sigma/E)^n\, \tilde{D} \quad ,$$

where γ is the matrix stacking fault energy, C is a constant, σ is the applied stress, and E is Young's modulus at the test temperature. The chemical diffusivity $\tilde{D}$ is given by

$$\tilde{D} = \tilde{D}_o\, \exp-\left(\frac{Q_{sd}}{RT}\right) \quad ,$$

where Q_{sd} is the activation energy for self-diffusion. This predicts that the activation energy for creep, Q_c, should be equal to Q_{sd}.

The experimentally determined creep parameters are listed below.

Alloy	Q_c, kcal/mole	n	m
Ni-1ThO$_2$	64	8.0	3.1 - 3.3
Ni-13.5Cr-1ThO$_2$	65	6.3	3.1 - 3.3
Ni-22.6Cr-1ThO$_2$	74	7.2	3.1 - 3.3
Ni-33.7Cr-1ThO$_2$	78	6.7	3.1 - 3.3

PART I. THE INFLUENCE OF INITIAL STRUCTURE ON TENSILE* AND CREEP DEFORMATION OF TD NICKEL

INTRODUCTION

It has been obvious for many years that dispersed second-phase particles can strengthen metals and alloys. With the discovery of SAP, TD Nickel, and DS Nickel, it became apparent that controlled thermomechanical processing of certain dispersion-hardened metals produced additional strengthening, which was retained even at very high temperatures, i.e., up to ~0.9 T_m, where T_m is the absolute melting temperature of the matrix. This excellent high temperature strength was derived from the fact that the "worked" structure was stable. That is, the particles helped to develop and/or pin the grain, subgrain, and dislocation structures during fabrication, such that recrystallization and grain growth were inhibited or effectively eliminated. Dispersion-strengthened metals with these structural characteristics have been referred to by Grant and Preston[5] as having a "high stored energy of cold work".

In order to help explain the added strengthening associated with thermomechanical processing, it has been suggested[6,7] that the strengthening effects of second-phase particles can be classified into two general categories:

CASE I. Strengthening by Direct Dislocation-Particle Interactions. Here the strengthening is caused by particles acting as barriers to dislocation motion during deformation, and the strength increase can usually be rationalized in terms of dislocation theories of dispersion hardening, e.g., Orowan bowing, cross-slip, climb, particle shearing, etc. This case is generally applicable to dispersion-strengthened single crystals and coarse-grained polycrystals.

CASE II. Indirect Particle Strengthening Effects. Here the particles serve to stabilize a fine grain size and/or subgrain structure produced during fabrication, and the total structure determines the dislocation mobility and defines the strength. This case often applies to commercial or semi-commercial dispersion-strengthened metals which have been thermomechanically processed such that they have a high stored energy of cold work. In such materials it is often impossible to relate the strengthening to dislocation theories of dispersion hardening.

Previous studies on high temperature creep of some experimental "recrystallized"** $Ni-ThO_2$ alloys[7,8] and TD Nickel bar[1] demonstrated these two cases. It was suggested that the rate-controlling creep process of the "recrystallized" alloys was the climb of edge dislocations over ThO_2 particles, an example of CASE I. However, for TD Nickel bar, an example of CASE II, no dislocation theory of creep could explain the experimental results. Here the chief mode of creep deformation was grain boundary sliding, but no physical model could explain the very high activation energy for creep, Q_c = 190 kcal/mole.

---

*The results of the tensile deformation studies have been presented at a recent conference and are in press, see Reference (4).

**It is difficult to give a uniformly accepted definition of "recrystallization" for dispersion-hardened metals. This arises because the recrystallized structure is not generally equiaxed as in pure metals or solid solution alloys, but retains some grain extension in the direction of working, thus resembling a worked structure (e.g., see Figure 2). The authors choose to define recrystallized dispersion-strengthened metals as those having a structure which contains undistorted annealing twins. This definition is of course applicable only to those FCC metals which form annealing twins. By this definition as-received TD Nickel bar is not recrystallized, whereas TD NiC ($Ni-20 Cr-2ThO_2$) sheet is at least partially recrystallized [see Reference (9)].

Other workers[10-15] have shown that the mechanical properties of Ni-ThO$_2$ alloys are sensitive to the amount and the type of thermomechanical processing; i.e., the state of grain, subgrain, and dislocation structure. The most extensive work to date along these lines is by Doble, et al.[15] They examined the influence of type of working operation and working direction on the mechanical properties and structural stability of TD Nickel bar, and concluded:

(a) <u>Cold swaging</u> produced strengthening at both room and elevated temperatures. TD Nickel specimens would not recrystallize even after swaging reductions of up to 95%.

(b) The degree of recrystallization and attendant mechanical properties produced by <u>cold rolling</u> and annealing depended on the rolling direction with respect to the initial bar axis.

(c) <u>Upset forging</u> and <u>torsional deformation</u> at room temperature lowered the elevated temperature strength in subsequent tensile tests.

In this phase of the work, the direct and indirect strengthening effects of second-phase particles have been examined by comparing the tensile deformation behavior of as-received TD Nickel bar with the same material which was cold rolled and recrystallized. The recrystallized material is found to be an example of CASE I, where the tensile deformation behavior could be rationalized in terms of a dislocation theory of dispersion hardening. On the other hand, the as-received TD Nickel is an example of CASE II, where a portion of the strengthening is associated with the fact that ThO$_2$ particles help promote the stable, fine, elongated grain structure during fabrication, i.e., a high stored energy of cold work. A comparison of the creep behavior of as-received and recrystallized TD Nickel was not fruitful from the point of view of quantitatively assessing the direct and indirect contributions of ThO$_2$ particles to creep strengthening.

EXPERIMENTAL PROCEDURES

Tensile deformation studies were made in an Instron at a strain rate of 1.67×10^{-4} sec^{-1} over the temperature range 25-1200°C. At temperatures above 300°C, the specimens were tested in vacuum. The specimen configurations used for both tensile and creep studies were as follows:

<u>As-received (bar)</u>: Threaded bar specimens were machined from 1/2-inch-diameter bar stock, and had the following dimensions: total length = 3 inches, gage length = 1 inch, gage diameter = 0.18 inch.

<u>Recrystallized (sheet)</u>: Sheet tensile specimens were machined from the final worked 0.020-inch-thick sheet prior to the recrystallization anneal. The overall length was 3-1/8 inches, with a gage length of 1 inch and a gage width of 1/4 inch. Gripping of both tensile and creep sheet specimens was accomplished by combined pin-loading and clamping with split serrated grips made from 1-inch-diameter TD Nickel bar.

Creep results on the as-received bar have been reported in Reference (1). In the present work, the conditions for testing the recrystallized sheet were identical with those used previously.[1] All tests were made in a vacuum of 10^{-5} torr under constant (tensile) stress conditions using a lever arm similar to that described by Fullman, et al.[16] Creep extension was measured optically with a sensitivity of 50-100 microinches by two sliding molybdenum strip extensometers scribed with fiducial marks, one on each side of the specimen gage length.

The preparation techniques for electron and optical microscopy have been described previously.[1, 17]

STRUCTURES OF THE MATERIALS

The TD Nickel used in this study was in the form of 1/2-inch-diameter bar, and the chemical analysis for impurities is given in Table 1. The as-received structure, shown in Figure 1, consists of fine, fibrous grains (~1 μ diameter by 10-15 μ long) elongated in the direction of the bar axis. This structure is stable even at very high temperatures, e.g., annealing for 3 hours at 1300°C caused no recrystallization, grain growth, or ThO_2 particle coarsening.[1] The material contained 2.3 vol % ThO_2, with a particle size range of ~100-1000 Å and an average particle diameter, $2\bar{r}_v$, of 370 Å. The mean planar center-to-center particle spacing, d, was calculated to be 2340 Å, from the following relation:

$$d^2 = \frac{8}{3\sum_i (f_i/r_{v_i}^2)} \quad , \tag{1}$$

where f_i = volume fraction of particles in a limited size range* having an average particle radius, r_{v_i}. The derivation of Equation (1) is given in the Appendix to Reference (1), and in all previous work the authors have used this formulation to calculate the particle spacing[1, 7, 8, 9]. This derivation is based on the assumption that the particles are arranged like the lattice points on an FCC lattice. The basic relation from which Equation (1) was derived was $d^2 = 4/\pi N_s$, where N_s is the number of particles intersecting a unit area[18].

TABLE 1. CHEMICAL ANALYSIS FOR IMPURITIES IN TD NICKEL
(Ni + 2.3 vol % ThO_2)[a]

Element	Wt %	Element	Wt %
S	0.006	Cu	0.002
P	<0.005	Ti	<0.001
Mn	0.01	Co	0.2
Si	0.001	Al	0.002
Fe	0.003	Ca	0.005
Mg	0.002		

(a) P and S were determined by wet chemical analysis, and all other elements by spectroscopy.

*A Zeiss Particle Size Analyzer was used to measure particle diameters from transmission electron micrographs. The Analyzer has 48 channels each representing a particular average size. However particles of a limited size range will register on each channel. For example, in Figure 15, particles denoted as being 160 Å in diameter include all particles in the size range ~146-174 Å.
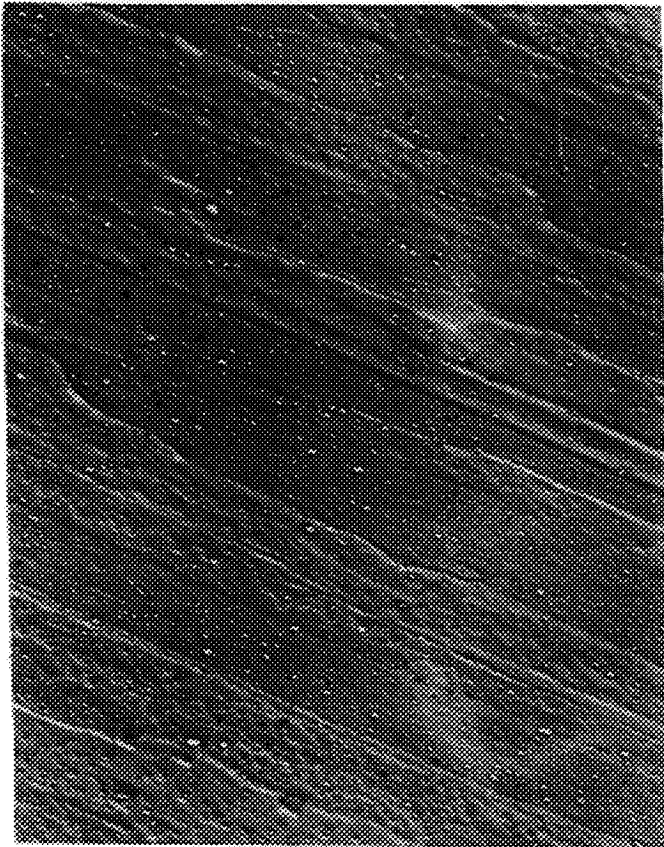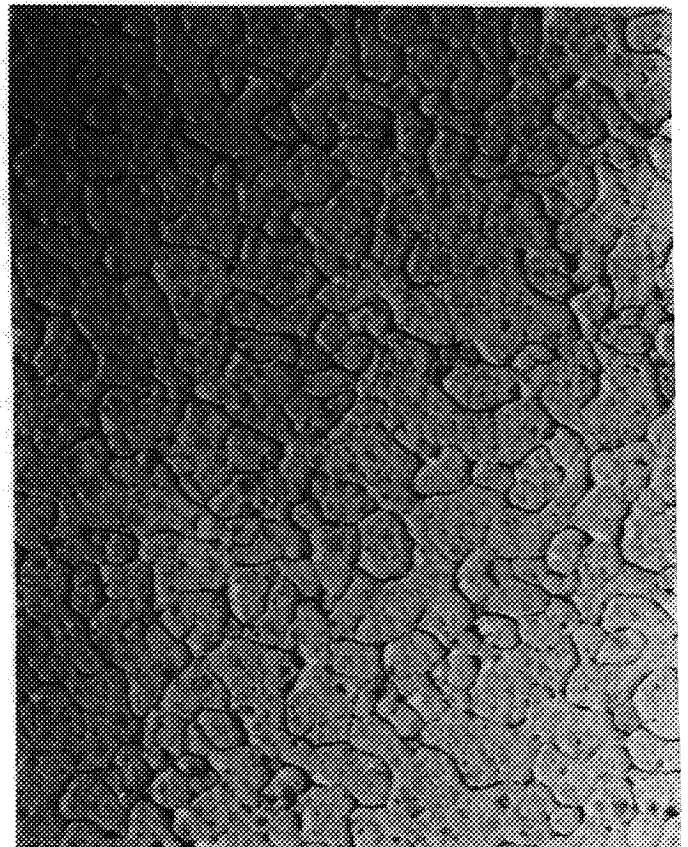
(a)   (b)

FIGURE 1. REPLICA ELECTRON MICROGRAPHS OF AS-RECEIVED
            TD NICKEL BAR, (a) PARALLEL TO BAR AXIS, 4800X,
            (b) TRANSVERSE TO BAR AXIS, 4800X

An alternative form is $d^2 = 1/N_s$, [18] which leads to the following relation when the particle size distribution is incorporated:

$$d^2 = \frac{2\pi}{3\sum_i (f_i / r_{vi}^2)} \quad .$$

(2)

When the particle data are treated using Equation (2), the calculated spacing is d = 2070 Å. This value is used in the portion of the report dealing with the Orowan stress calculation in order to be consistent with Ashby's[19] derivation of the Orowan stress [see Equation (5a)].

The structure of the recrystallized TD Nickel is shown in Figure 2. This structure, which consists of coarse, somewhat elongated grains and a high density of fine annealing twins, was produced in the following way:

(1) Two flat parallel surfaces were machined on longitudinal sections of the 1/2-inch-diameter bar.

(2) The specimen blanks were first cold rolled 43%, perpendicular to the original bar axis. They were then rotated 90 degrees and cold rolled parallel to the original bar axis to 0.020-inch-thick sheets, giving a total reduction of 95%.

(3) Specimens for tensile and creep testing were machined such that their axes were parallel to the original bar axis and the final rolling direction.

(4) All specimens were then vacuum annealed for 3 hours at 1300 °C.

Figure 3 compares transmission electron micrographs of the as-received and recrystallized materials. No evidence was found to indicate that the cold rolling caused any ThO_2 particle deformation or fracture or any decohesion at particle-matrix interfaces. Decohesion and resultant void formation have been reported previously for deformed TD NiC sheet.[20,21] Although no quantitative measurements were made, it appeared that the average dislocation density in the recrystallized material was slightly less than in the as-received bar.

RESULTS AND DISCUSSION

Tensile Deformation Studies

The influence of temperature on the yield and ultimate tensile strength of as-received and recrystallized TD Nickel is illustrated in Figure 4, and all pertinent data are listed in Table 2. Also included in Figure 4 are data from the literature showing the yield strength of pure polycrystalline nickel, from room temperature to 1200 °C. It is seen that, over the entire temperature range, the recrystallized TD Nickel has a higher yield strength than pure nickel. Furthermore, there is an additional increment in yield strength in the case of as-received TD Nickel bar. The recrystallized material work hardened to give the same ultimate strength as the as-received TD Nickel over the temperature range 25-300 °C. However, at higher temperatures the ultimate strength of the recrystallized material decreased more rapidly with increasing temperature.

FIGURE 2. OPTICAL MICROGRAPHS OF RECRYSTALLIZED TD NICKEL, 100X

Section C
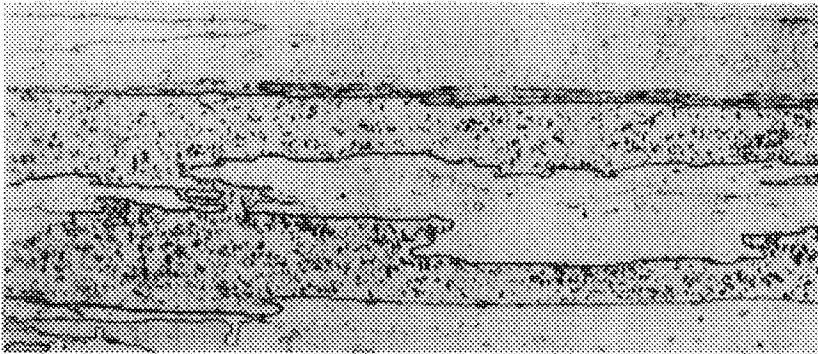
Section A

Section B

Original Bar Axis and Final
Rolling Direction
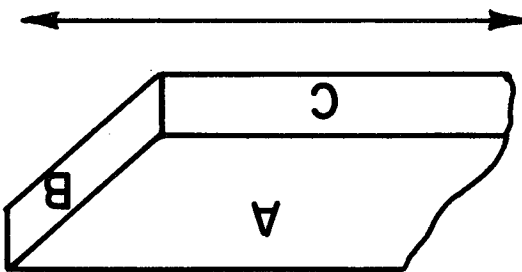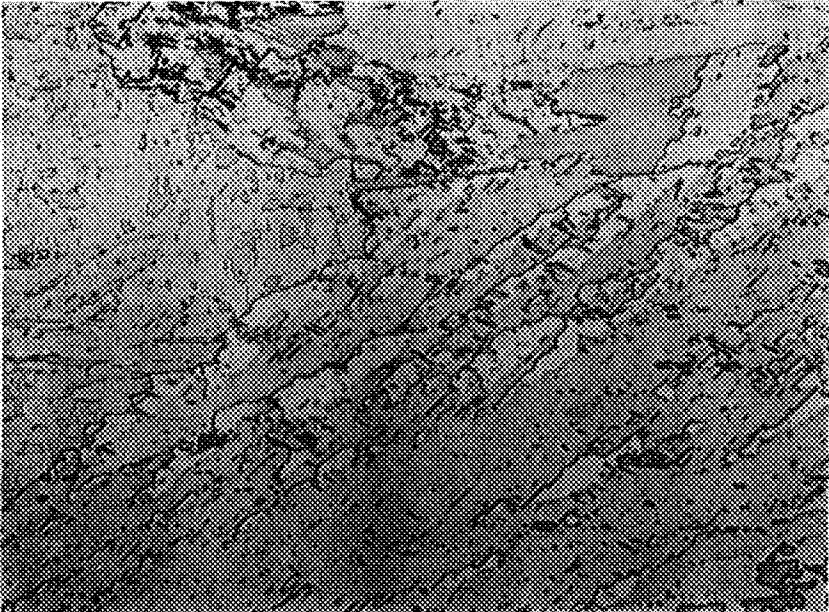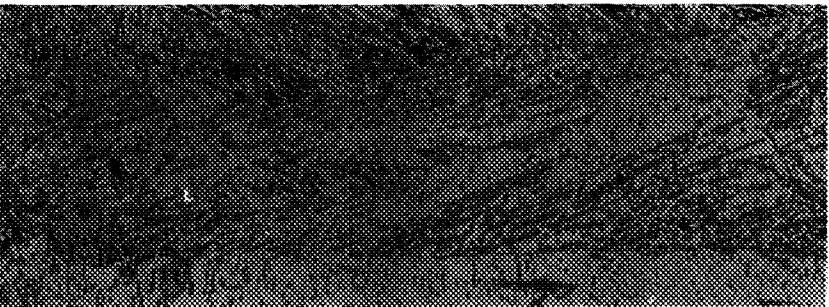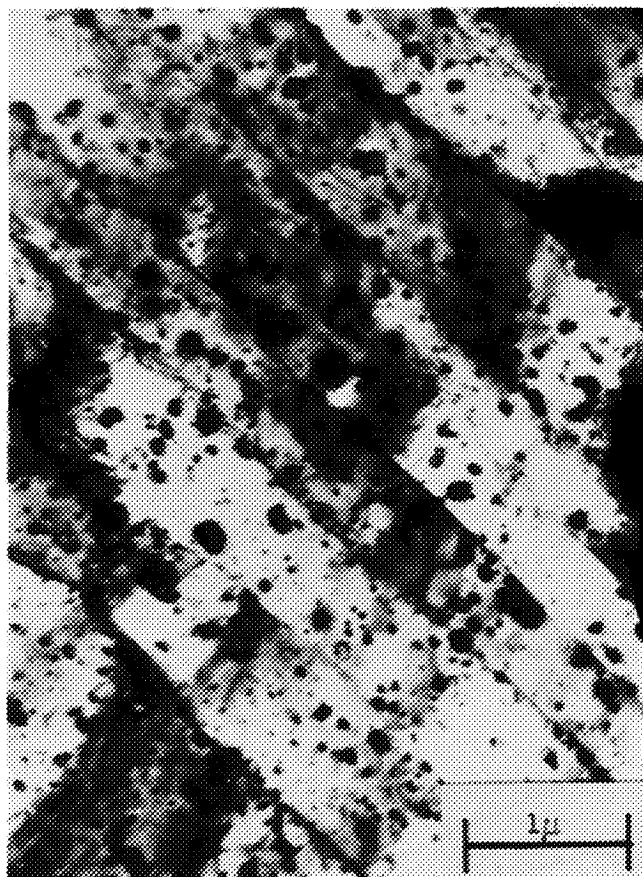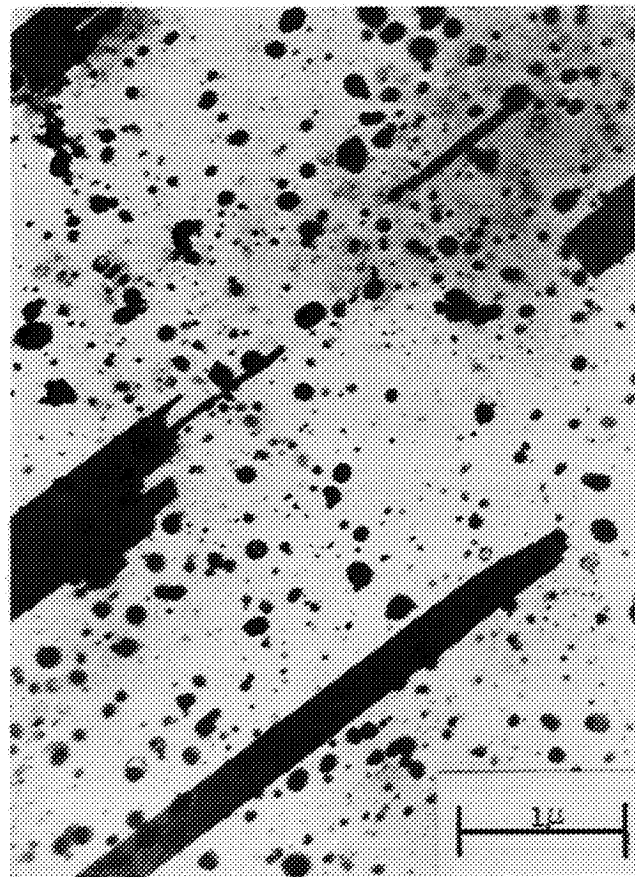
(a)   (b)

FIGURE 3.   TRANSMISSION ELECTRON MICROGRAPHS, (a) AS-RECEIVED
            TD NICKEL BAR, (b) RECRYSTALLIZED TD NICKEL
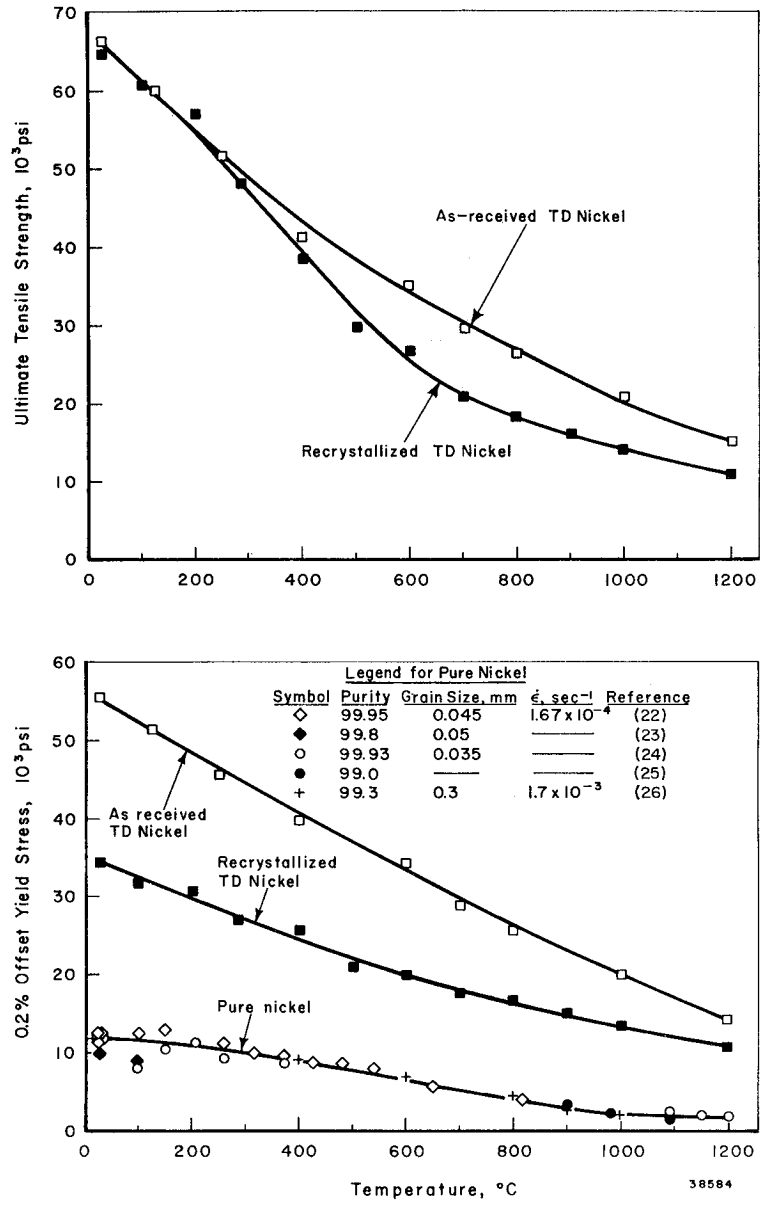
FIGURE 4. TEMPERATURE DEPENDENCE OF THE YIELD AND ULTIMATE
STRENGTHS OF AS-RECEIVED AND RECRYSTALLIZED
TD NICKEL

TABLE 2. TENSILE DATA FOR AS-RECEIVED AND RECRYSTALLIZED TD NICKEL TESTED AT $\dot\epsilon = 1.67 \times 10^{-4}$ SEC^{-1}

Test Temperature, °C	Stress, psi, at				Uniform Elongation, %	Total Elongation, %	Reduction in Area, %
	0.2% ϵ	2% ϵ	5% ϵ	UTS			
As-Received Bar							
25	55,600	62,300	66,000	66,300	8.0	20.5	90.1
125	51,500	57,200	59,800	60,000	6.6	19.2	91.3
250	45,500	49,800	51,300	51,300	6.6	20.3	91.0
400	39,800	41,300	--	41,300	2.0	13.4	91.4
600	34,200	--	--	35,100	1.2	8.6	71.7
700	28,100	--	--	29,400	1.8	9.6	63.0
800	25,700	--	--	26,300	0.7	5.6	40.8
1000	20,100	--	--	20,700	0.7	2.4	18.2
1200	14,200	--	--	15,100	0.8	1.5	3.0
Recrystallized (Sheet)							
25	34,300	45,700	57,500	64,800	15.2	16.2	--
100	31,500	43,900	54,500	60,800	13.1	14.3	--
200	30,800	42,000	51,500	57,200	11.4	12.2	--
285	26,900	37,700	44,800	47,700	12.0	13.6	--
400	25,800	32,500	35,700	38,500	15.4	17.2	--
500	20,800	25,000	27,000	29,700	14.1	15.3	--
600	19,900	23,900	25,700	26,600	13.0	14.6	--
700	17,500	19,900	20,800	20,800	5.3	7.8	--
800	16,600	18,100	18,300	18,300	5.7	9.0	--
900	15,000	--	--	16,100	0.9	2.9	--
1000	13,200	--	--	14,400	1.0	3.8	--
1200	10,600	--	--	10,900	0.7	2.0	--

The temperature dependence of the ductility is shown in Figure 5. The two materials exhibit no significant difference in total elongation. The rapid decrease in reduction in area of as-received TD Nickel bar at ~600 °C has been observed previously.[1, 11, 27] The lower reduction in area values at high temperatures are associated with a change in the fracturing process. At temperatures ≳600 °C, grain boundary voids form as the tensile specimen starts to neck.[17] Fracture occurs by internal necking and merging of the voids, which results in a lower measured (macroscopic) ductility.
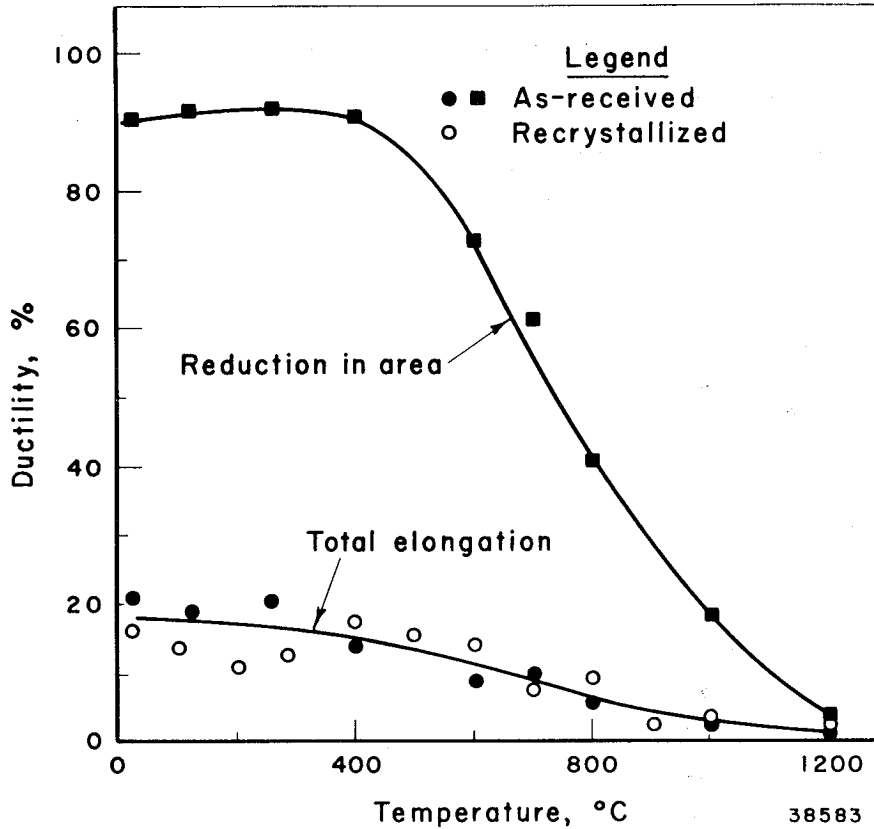
FIGURE 5. TEMPERATURE DEPENDENCE OF THE TENSILE DUCTILITY
OF AS-RECEIVED AND RECRYSTALLIZED TD NICKEL

The dislocation structure in a deformed specimen of the recrystallized material is shown in Figure 6. Pronounced tangling is evident, and the cell walls seem to be anchored by the larger ThO_2 particles, as has been shown previously by von Heimendahl and Thomas[13].

The yield strength data in Figure 4 can be treated to show that recrystallized TD Nickel is an example of CASE I, whereas the as-received TD Nickel is an example of CASE II, as defined earlier. The ultimate strength results are not considered here in these terms because of the complicating factors of work hardening and elevated temperature fracturing.

In the recrystallized material, the strengthening due to ThO_2 particles can be examined by means of various theories: (a) Ansell's theory of stress-induced particle shear or fracture[6] and (b) Ashby's reformulation of the Orowan theory of hardening by nondeforming particles[19].

In Ansell's model the shear yield strength, τ, of a dispersion-strengthened alloy containing fine, noncoherent particles is:

$$\tau \approx \frac{G_p (2r_s)}{4 K (d - 2r_s)} \quad , \tag{3}$$

where: G_p = shear modulus of the particle at the test temperature

$2r_s$ = 300 Å = $\sqrt{2/3}$ $(2r_v)$ = average <u>planar</u> particle diameter

d = 2070 Å = mean <u>planar</u> center-to-center particle spacing [from Equation (2)]

K = constant, $\simeq$ 30 for defect-free particles.

Wygant[28] has reported shear modulus values for ThO_2 over the temperature range 30-1300°C. Using these data, the calculated values of τ from Equation (3) are compared in Figure 7 with the experimental shear yield stress data for recrystallized TD Nickel. Here τ (experimental) was taken as $\sigma/2$, where σ is the tensile yield strength from Figure 4. Figure 7 shows that the calculated (dashed) curve predicts shear yield stress values 3,000-7,000 psi higher than the observed yield stress of recrystallized TD Nickel. However, the slope of the calculated curve is in rough agreement with that of the experimental results.

The revised Orowan model due to Ashby[19] gives the shear yield strength of a metal containing hard particles as:

$$\tau = \tau_s + \tau_p \quad , \tag{4}$$

where τ_s is the matrix shear strength, and τ_p (the Orowan stress) is the stress increment necessary to cause a dislocation to bow between particles and pinch off. Ashby's calculation for τ_p gives:

$$\tau_p(\text{edge}) = \left(\frac{1}{1.18} \right) \left(\frac{G_m b}{2\pi} \right) \left(\frac{1}{d - 2r_s} \right) \ln \left(\frac{r_s}{b} \right) \tag{5a}$$

$$\tau_p(\text{screw}) = \left(\frac{1}{1-\nu} \right) \tau_p(\text{edge}) \quad , $$

where: b = Burgers vector

ν = Poisson's ratio

G_m = Shear modulus of matrix at the test temperature*.

---

*Susse's[29] shear modulus data for nickel, from 25-1000°C, were used for these calculations. It was necessary to extrapolate these results in the temperature range 1000-1200°C (see Figure A-1, Appendix).
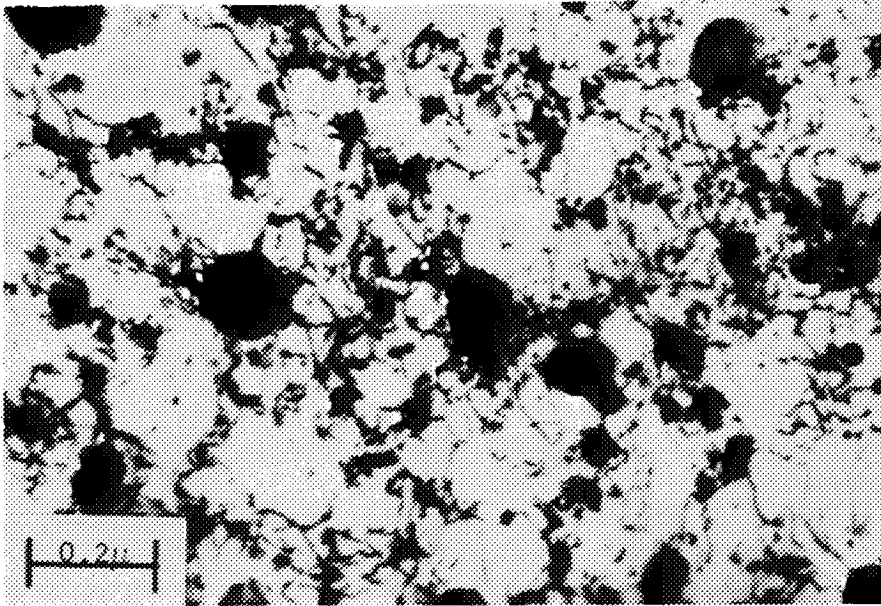
FIGURE 6. DISLOCATION STRUCTURE IN RECRYSTALLIZED TD NICKEL,
DEFORMED TO 13% ϵ IN TENSION AT 100°C
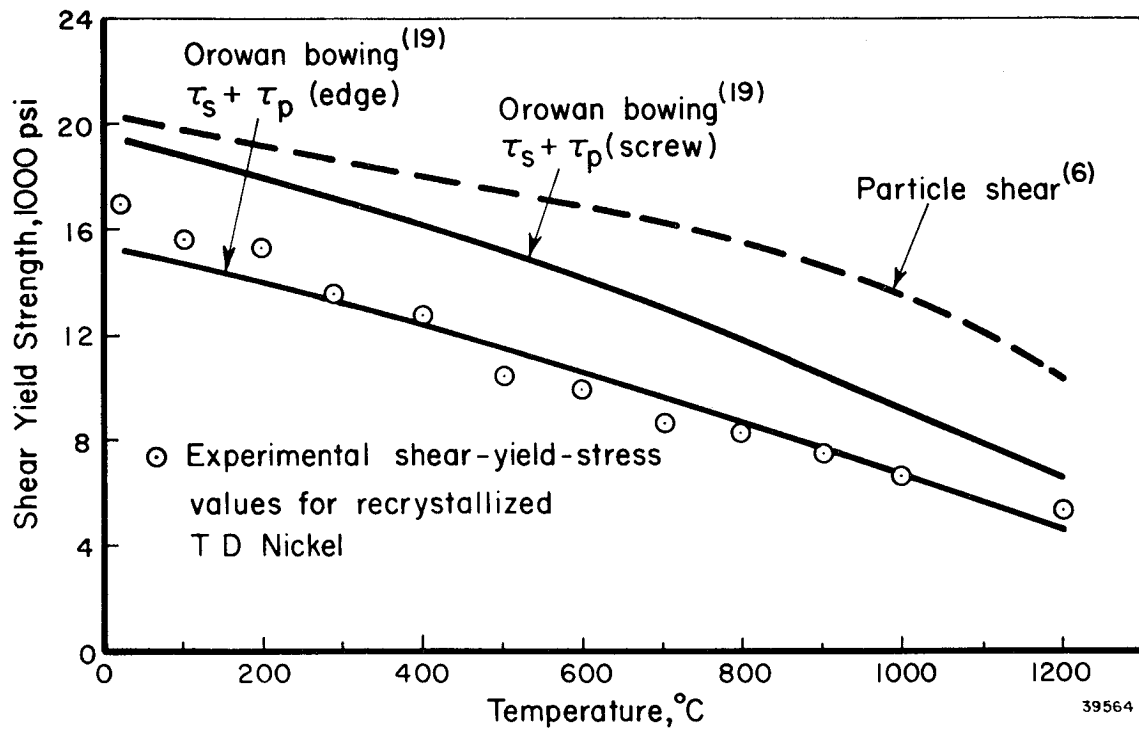
FIGURE 7. COMPARISON OF EXPERIMENTAL YIELD (SHEAR) STRESS OF
RECRYSTALLIZED TD NICKEL WITH PREDICTIONS OF THE
OROWAN THEORY (SOLID CURVES), AND THE PARTICLE
SHEAR THEORY (DASHED CURVE)

The good agreement between τ(experimental) and the calculated values of $\tau_s + \tau_p$(edge) is shown in Figure 7. Here τ_s represents the yield strength of pure polycrystalline nickel taken from Figure 4, and was converted to shear stress by the relation $\tau_s = \sigma/2$. The experimental results in Figure 7 agree better with the Orowan theory than with the particle shearing theory. Thus, in the present case it appears more likely that the Orowan mechanism is operative for recrystallized TD Nickel. These results are in accord with the findings of von Heimendahl and Thomas[13], who discussed the room temperature yield strength of recrystallized TD Nickel in terms of the Orowan strengthening mechanism.

However, the yield strength of as-received TD Nickel must include an additional (empirical) term, such that:

$$\tau = \tau_s + \tau_p + \tau_{se} \quad , \tag{6}$$

where τ_{se} is related to the strength increase caused by the fine stable grain and sub-grain structure, and can be thought of phenomenologically as the "stress increment due to the stored energy of cold work". More specifically, τ_{se} could be strengthening associated with the very fine grain size, a higher initial dislocation density than in the recrystallized material or a texturing effect.

It is possible to get an approximate estimate of the grain size effect by considering the results in Figure 8. Here the room temperature grain size dependence of the initial flow stress of polycrystalline nickel is shown in the usual Petch-type plot, where ℓ in Figure 8 is the average grain diameter. A very long extrapolation to the effective grain size of TD Nickel bar* indicates an initial flow stress value of ~16,000 psi. An exact measure of the grain size of recrystallized TD Nickel is difficult (see Figure 2). However, a reasonable estimate would correspond to $\ell^{-1/2}$ values of 0.1 to 0.3 $\mu^{-1/2}$. From Figure 8 the initial flow stresses at these grain sizes would be 3000-7000 psi. Therefore, the room temperature strength increment in as-received TD Nickel due to the grain size effect would be 9000-13,000 psi. However, from Figure 4, it is seen that the room temperature yield strength of as-received TD Nickel is ~21,000 psi greater than that of the recrystallized material. Thus the grain size effect can account for only about 1/2 of τ_{se}. As noted above, the remaining portion of τ_{se} could be associated with a higher dislocation density in the as-received TD Nickel or a difference in texture between as-received and recrystallized materials. However, at present, it is not possible to discuss these effects quantitatively since the appropriate measurements have not been made.

Creep Studies

In a previous paper[7] the authors compared the steady-state creep behavior of TD Nickel bar with that of some experimental "recrystallized" Ni-ThO$_2$ alloys which had been prepared by Sherritt Gordon Mines, Ltd. These experimental alloys were not Sherritt Gordon's commercial DS Nickel, and they had not been thermomechanically processed to have optimum high temperature strength. Table 3 shows that the creep strength of TD Nickel bar was much superior to a Ni-ThO$_2$ alloy which had a similar particle size and spacing, but which did not have the same fine grain and subgrain structure.

---

*During tensile tests the fiber axis of the elongated grains (avg. grain dia. = 1.1 μ) was parallel to the stress axis. The effective grain size is taken as the spacing between boundaries on a plane at 45° to the tensile axis; i.e., ℓ (eff) ≈ 1.6 μ.
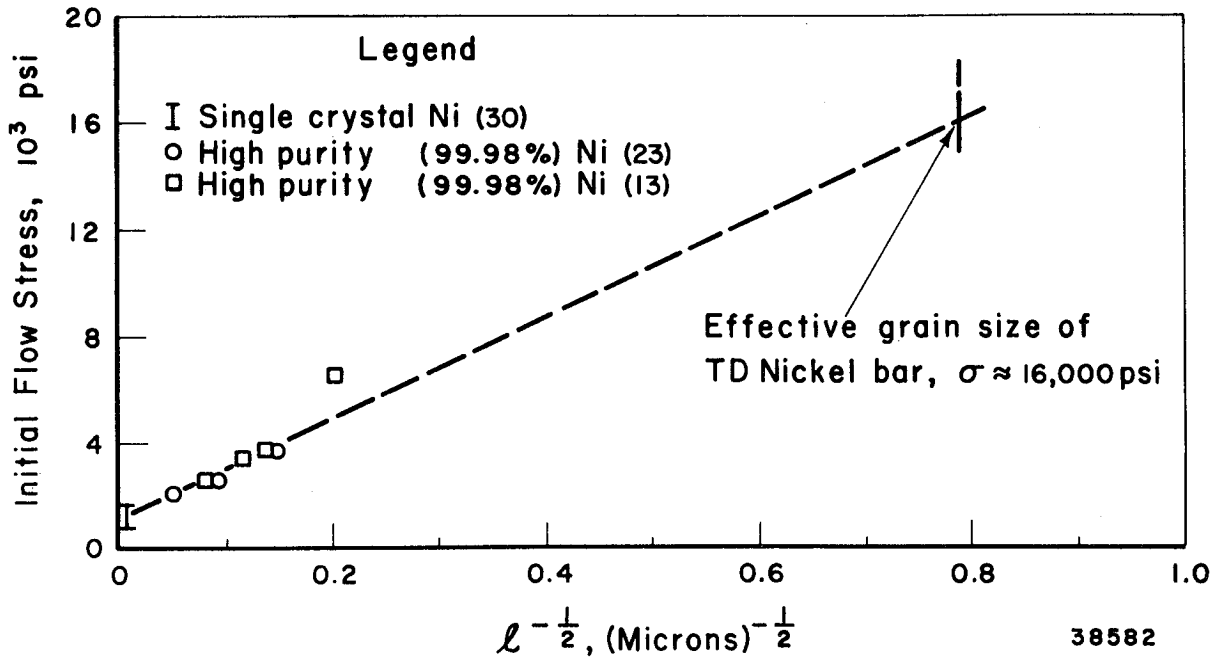
FIGURE 8. GRAIN SIZE DEPENDENCE OF THE ROOM TEMPERATURE INITIAL FLOW STRESS OF PURE NICKEL

TABLE 3. COMPARISON OF "CREEP STRENGTH" OF TD NICKEL BAR[1] WITH THAT OF A "PARTIALLY RECRYSTALLIZED" EXPERIMENTAL ALLOY[7]

	Particle Spacing, d, Å	Avg Particle Diam., $2r_V$, Å	Stress to Give $\dot{\epsilon}_s = 1.2 \times 10^{-7}$ sec^{-1} at 900°C
TD Nickel bar (2.3 vol % ThO_2)	2340[a]	370	20,320
Experimental partially recrystallized Ni-ThO_2 alloy (2.56 vol % ThO_2)	1760[a]	219	12,590

(a) Here d was calculated from Equation (1).

From these results it was concluded that TD Nickel bar exhibited an additional (indirect) strengthening increment in creep. The present study on creep of recrystallized TD Nickel was thus undertaken with the aim of obtaining a quantitative comparison of the influence of initial structure on the steady-state creep rate. Since the particle size and spacing were not affected by working and annealing, a direct comparison with as-received TD Nickel bar could be obtained, with the only variables being the grain and subgrain size and dislocation density and distribution.

The recrystallized TD Nickel was tested in creep over the stress range 9000-18,000 psi and temperature range 650-1000°C, and the results are given in Table 4. A typical creep curve is shown in Figure 9. As is the case for other Ni-ThO_2 alloys[1, 7-9], the total creep strains were quite small (~1-3% total elongation at fracture). The fractures were predominately intergranular. In several specimens which contained small regions of unrecrystallized material, voids formed at the interface between the recrystallized and unrecrystallized areas (see Figure 10).

TABLE 4.   STEADY-STATE CREEP RATE OF RECRYSTALLIZED TD NICKEL
AS A FUNCTION OF TEMPERATURE AND APPLIED STRESS

σ, psi	T, °C	$\dot{\epsilon}_s$, sec^{-1}	σ, psi	T, °C	$\dot{\epsilon}_s$, sec^{-1}
18,000	725	(a)	13,000	950	2.14×10^{-7}
17,300	650	1.39×10^{-8}	13,000	925	4.17×10^{-9}
17,000	950	(a)	12,000	975	9.93×10^{-9}
16,000	725	1.78×10^{-8}	12,000	960	7.50×10^{-10}
16,000	715	2.78×10^{-8}	12,000	950	1.25×10^{-9}
16,000	700	1.28×10^{-9}	12,000	925	1.53×10^{-10}
14,000	860	1.95×10^{-8}	11,000	950	6.80×10^{-10}
14,000	825	3.77×10^{-10}	9,000	1000	1.08×10^{-9}
14,000	815	2.00×10^{-10}			

(a) Failed on loading; no creep curve obtained.

The temperature dependence of the steady-state creep rate at three applied stress levels is illustrated in Figure 11, and similar results for as-received TD Nickel bar [from Reference (1)] are shown in Figure 12 for comparison. The creep results for the recrystallized material showed considerably more scatter than those of the as-received bar. In Figure 11, three parallel lines were drawn, which best fit the creep data at each of the three applied stress levels. The calculated activation energy for creep was Q_c = 235 kcal/mole, which is somewhat higher than that of the as-received TD Nickel bar (Q_c = 190 kcal/mole). These high activation energies for creep cannot, at present, be rationalized in terms of any rate-controlling creep process. In view of the fact that Q_c for "recrystallized" experimental Ni-ThO_2 alloys was equal to the activation energy for self-diffusion in Ni[8] (64 kcal/mole), it is very surprising that such a high activation energy for creep was obtained for the recrystallized TD Nickel. These results are consistent, however, with the findings of Doble et al.[15] They calculated activation energies from tensile deformation results on TD Nickel bar and recrystallized TD Nickel, and obtained the following values:

(a) TD Nickel bar, Q = 160-220 kcal/mole, at ~1100°C
(b) recrystallized TD Nickel, Q = 190-330 kcal/mole, at ~1100°C.
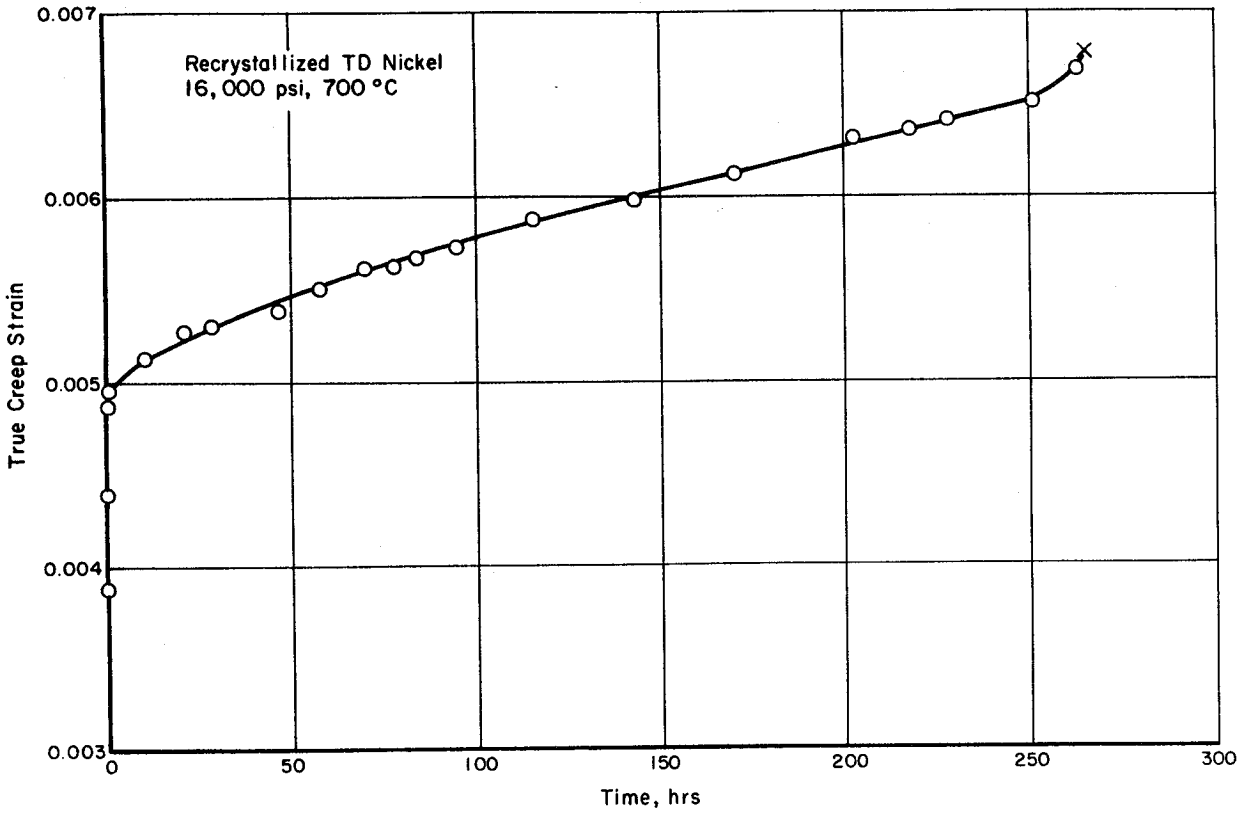
FIGURE 9. TYPICAL CREEP CURVE FOR RECRYSTALLIZED TD NICKEL
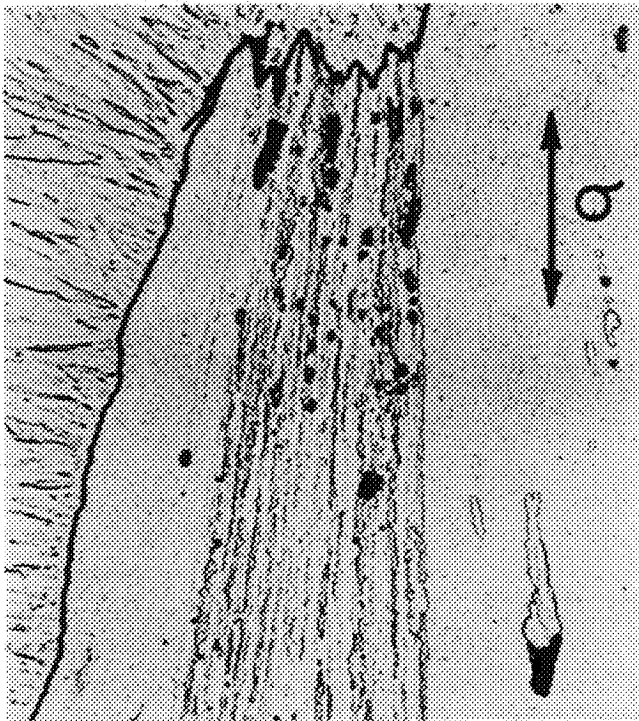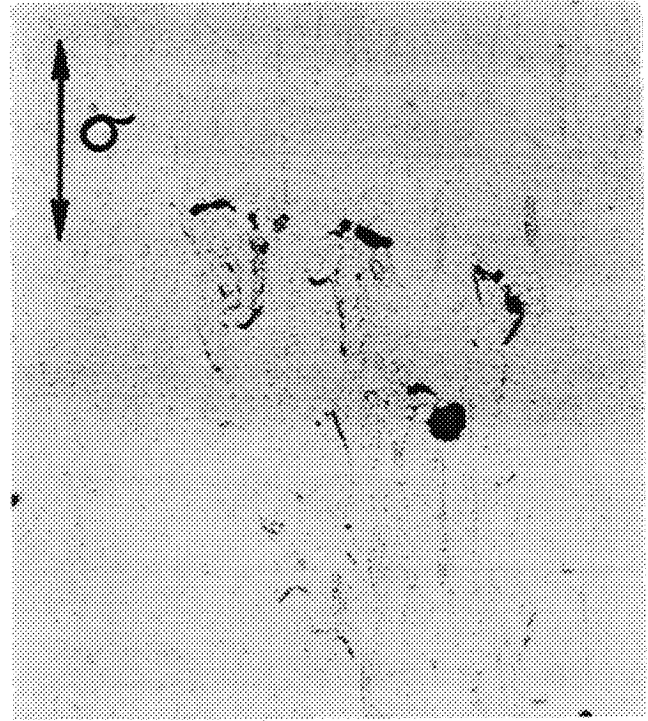
(a)   (b)

FIGURE 10. RECRYSTALLIZED TD NICKEL CREPT TO FRACTURE AT
            σ = 12,000 PSI, T = 925°C

            Note voids formed at interface between recrystallized matrix
            and patches of unrecrystallized material, (a) sheet thickness,
            Ni plated, 600X, (b) plane of sheet, 600X.
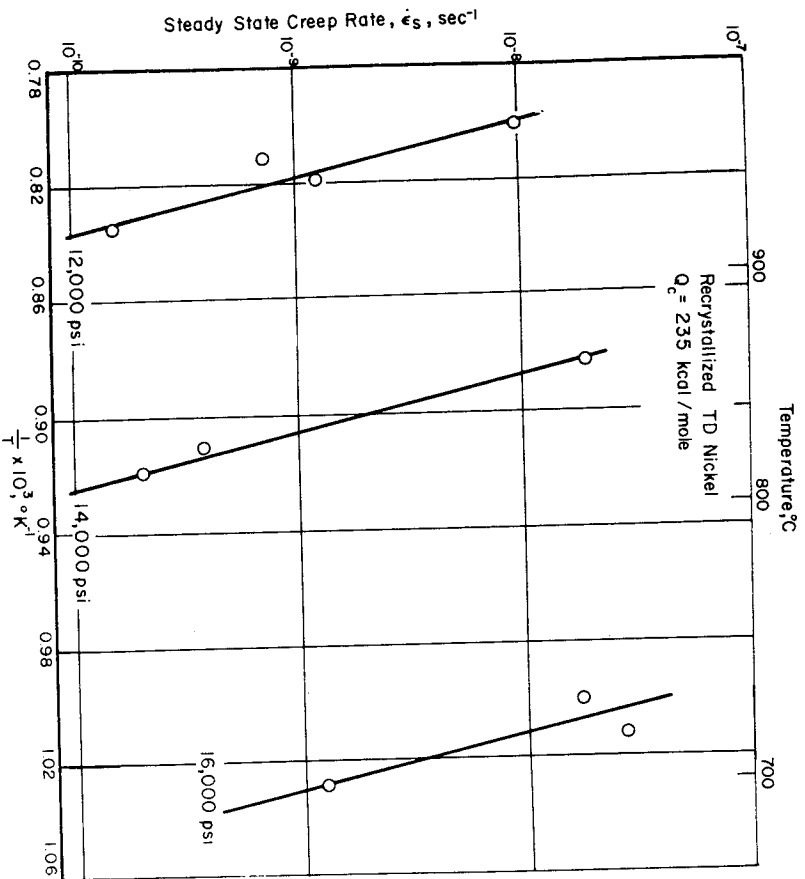
FIGURE 11. TEMPERATURE
DEPENDENCE OF THE
STEADY-STATE CREEP
RATE OF RECRYSTALLIZED
TD NICKEL
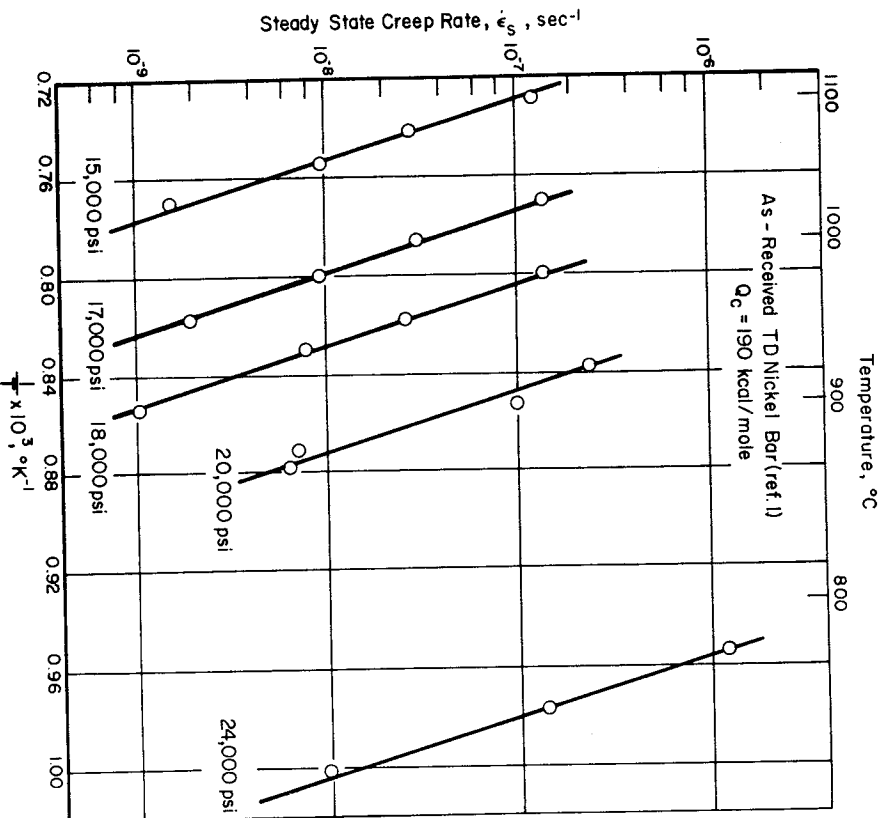
FIGURE 12. TEMPERATURE
DEPENDENCE OF THE
STEADY-STATE CREEP
RATE OF AS-RECEIVED TD
NICKEL BAR [FROM
REFERENCE (1)]

20

The stress dependence of the steady-state creep rate, $\dot{\epsilon}_s$, can be empirically represented by $\dot{\epsilon}_s \propto e^{B\sigma}$ or $\dot{\epsilon}_s \propto \sigma^n$, as shown in Figures 13 and 14, respectively. In both plots, there is a break in the curve for the recrystallized material, which indicates a different stress dependence of the temperature-compensated creep rate at low and high stresses. However, this apparent effect might also be caused in part by a stress-dependent or temperature-dependent activation energy. The results in Figure 11 cover the stress range 12,000-16,000 psi. It is possible that at lower stresses, say $\sigma \lesssim 11,000$ psi, or at higher temperatures, say $T \gtrsim 950\,°C$, a different experimental value of Q_c would be obtained. Other empirical formulations[52] of the stress dependence of $\dot{\epsilon}_s$, such as $\dot{\epsilon}_s \propto K'[\sinh(\alpha\sigma)]^n$, would probably fit the results as well as the exponential and power laws. However, the present data were not plotted in this fashion.

It was not possible to make any extensive direct comparison of the creep properties of as-received bar with those of the recrystallized material. Since the TD Nickel bar was so much stronger, it was impossible to select a given stress and temperature which would allow a direct comparison to be made conveniently. For example, at 950°C and 17,000 psi a specimen of as-received TD Nickel bar failed after 354 hours, whereas a recrystallized specimen failed immediately on loading. In order to compare steady-state creep rates it was necessary to calculate $\dot{\epsilon}_s$ from the data in Figure 13. These values are given in Table 5 and, if taken literally, would indicate that at a given stress and temperature the creep rates of as-received bar are $\sim 10^{10} - 10^{15}$ times lower than those of recrystallized material. These figures are probably not realistic, but they do serve to indicate that recrystallization does greatly increase the steady-state creep rate of TD Nickel.

TABLE 5. COMPARISON OF CREEP PROPERTIES OF AS-RECEIVED AND RECRYSTALLIZED TD NICKEL

	T, °C	σ, psi	$\dot{\epsilon}_s$, sec^{-1}	t_r, hr
As-Received	950	17,000	1.96×10^{-9}	353.6
Recrystallized	950	17,000	$(3.99 \times 10^{+6})$[a]	Failed on loading, no creep curve obtained
As-Received	700	16,000	(3.6×10^{-19})[a]	?
Recrystallized	700	16,000	1.28×10^{-9}	265.9

(a) Calculated from Figure 13. These, of course, are artificial values and are probably not physically realistic.
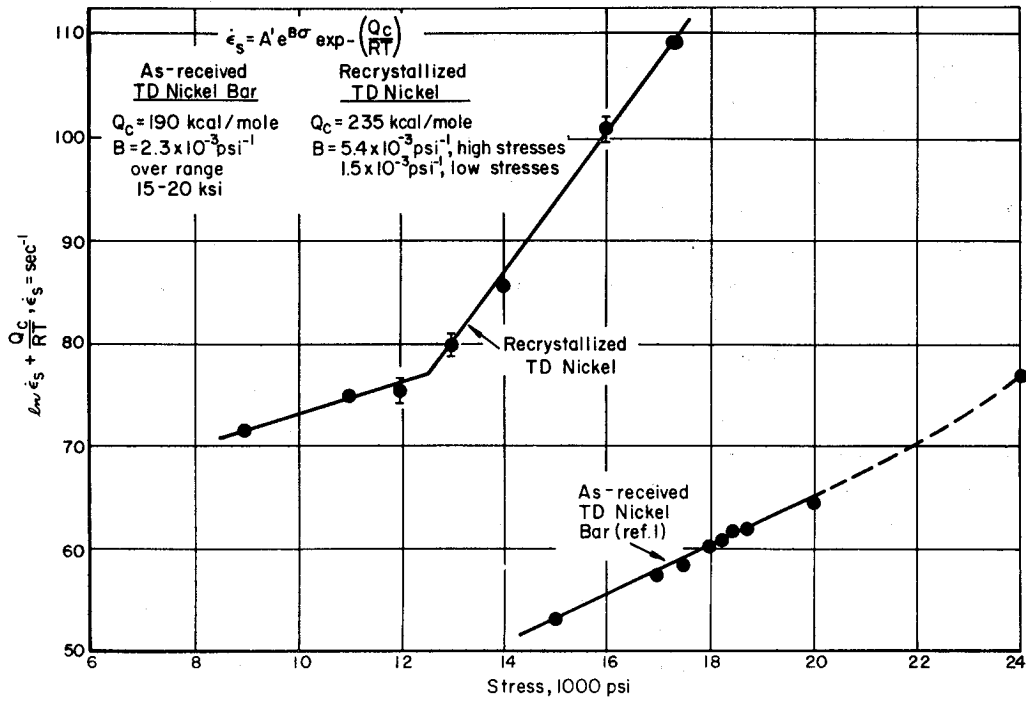
FIGURE 13. TEMPERATURE-COMPENSATED CREEP RATE AS A FUNCTION
OF APPLIED STRESS, PLOTTED ACCORDING TO THE
RELATION $\dot{\epsilon}_s \propto e^{B\sigma}$
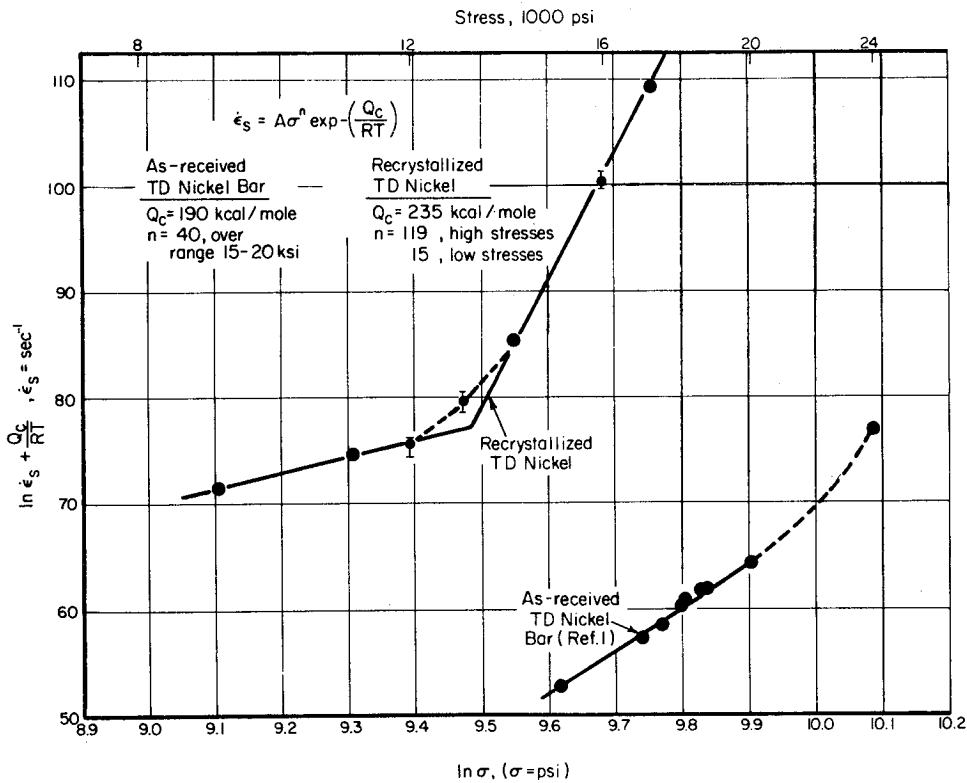
FIGURE 14. TEMPERATURE-COMPENSATED CREEP RATE AS A FUNCTION
OF $\ln \sigma$, PLOTTED ACCORDING TO THE RELATION $\dot{\epsilon}_s \propto \sigma^n$

PART II. THE EFFECT OF MATRIX STACKING FAULT ENERGY ON CREEP OF Ni-Cr-ThO$_2$ ALLOYS

INTRODUCTION

Commercial suppliers of dispersion-strengthened nickel alloys have added Cr as an alloying element (normally ~20 wt %) in order to improve the oxidation resistance. Another effect of Cr is to lower the stacking fault energy of Ni.[31, 32] Thus, it is likely that the high temperature deformation behavior of Ni-ThO$_2$ alloys would be altered by Cr additions. For example, dislocation cross-slip and climb should be more difficult for Cr-containing alloys, and in fact several previous studies[33, 34] have shown that in binary Ni-Cr alloys the steady-state creep rate decreases as the Cr content increases. Thus, this part of the research program was undertaken to study how lowering the stacking fault energy of Ni by controlled additions of Cr influences the high temperature creep behavior of Ni-Cr-1ThO$_2$ alloys.

There have been several reports in the literature that decreasing the stacking fault energy, γ, of FCC metals and alloys causes a decrease in the high temperature steady-state creep rate, $\dot{\epsilon}_s$. This has been demonstrated for pure FCC metals[2], α-brasses[3], Ni-Co alloys[35], and Ni-Cr alloys[33, 34]. Sherby and co-workers[2, 3] have determined quantitatively the magnitude of the decrease in $\dot{\epsilon}_s$ with decreasing γ, and have treated their results by the following equation:

$$\dot{\epsilon}_s = C\gamma^m(\sigma/E)^n \tilde{D} \quad . \tag{7}$$

Here σ is the applied stress, E is Young's modulus at the test temperature, C is a constant, and $\tilde{D}$ is the chemical diffusivity. Since $\tilde{D} = \tilde{D}_o \exp-(Q_{sd}/RT)$, where Q_{sd} is the activation energy for self-diffusion, then for Equation (7) to hold, the activation energy for creep should equal Q_{sd}. This was the case for pure FCC metals and α-brasses, and for both cases the exponents in Equation (7) were: m = 3.5 and n ≈ 5.

Weertman[36] has explained the influence of γ on $\dot{\epsilon}_s$ by means of a dislocation climb model. He assumed that the rate of dislocation core diffusion is much smaller in partial dislocations (low γ) than in perfect dislocations (high γ). This leads to a lower dislocation climb rate in low stacking fault energy alloys, which in turn results in a lower steady-state creep rate. However, recently Birnbaum, et al.[37], presented some experimental results which show that Weertman's assumption about relative core diffusivities may be incorrect. Birnbaum, et al. studied self-diffusion of Ni^{63} along edge dislocations in single crystals of Ni [γ = 240 erg/cm$^{2(32)}$] and Ni-60Co [γ = 30 erg/cm$^{2(31)}$]. Over their experimental temperature range (500-600 °C), they found that the core diffusivity in Ni-60Co was faster than in pure Ni, i.e., the opposite of what Weertman assumed. It thus appears that further examination of the details of Weertman's climb model may be necessary.

EXPERIMENTAL PROCEDURES

The methods used in creep testing the Ni-Cr-ThO$_2$ alloys were identical to those described on page 5, for the TD Nickel. The materials were in sheet form, 0.020 inch thick, and the specimen configuration was the same as that of the recrystallized TD Nickel sheet. Metallographic procedures and thinning techniques for electron micros- copy were identical to those reported in Reference (9). Since the creep tests were in vacuum, it was essential to determine that the composition did not change during creep as a result of evaporation of Cr, which has a high vapor pressure. Several chemical analyses on crept specimens showed that, under the test conditions employed, no significant Cr losses occurred.

STRUCTURES OF THE MATERIALS

Three Ni-Cr-1 vol % ThO$_2$ alloys, having Cr contents of 13.5, 22.6, and 33.7 wt %, were prepared by Sherritt Gordon Mines, Ltd. in the form of 0.020-inch-thick "recrystallized" sheet. The fabrication treatment employed cross rolling, intermittent anneals at 1200°C, and a final 1/2-hour anneal at 1200°C. This treatment was designed to produce similar "recrystallized" structures in each of the alloys, with no direction- ality or mechanical anisotropy in the final sheets. Each alloy contained ~1 vol % ThO$_2$ with average particle diameters of ~150-200 Å. This ThO$_2$ composition and particle size were chosen so that the creep results could be compared with those from a pre- vious study[7, 8] on a "recrystallized" Ni-1 vol % ThO$_2$ alloy.*

Chemical analysis results for impurity elements in the experimental alloys are given in Table 6, and the ThO$_2$ particle sizes and spacings are compared in Table 7. In Table 7 it is noted that all four alloys have reasonably similar average particle sizes and spacings. As in previous work by the authors[1, 7-9], the mean planar center-to- center particle spacing, d, was calculated from Equation (1), using the size distribution plots in Figure 15. The distributions in Figure 15 were obtained by measuring 900-1000 particle diameters per alloy from transmission electron micrographs, using a Zeiss Particle Size Analyzer.

Since the main aim of this study was to assess the effect of stacking fault energy on the steady-state creep rate, it was important to assure that the initial structure of the alloys were similar. Marked variations in grain size, substructure, and particle size and spacing from one alloy to another could obscure the effects of γ on the creep behavior. Therefore, a careful examination of the structures of the as-received alloys was made using both optical microscopy and transmission electron microscopy.

The initial structures of the four alloys are compared in Figures 16-18. Figure 16 shows that in the planes of the sheets the four alloys have very similar structures (e.g., grain size, twin density, etc.). In the sheet thickness direction, Figure 17, the four alloys also appear to be similar, with the possible exception of the Ni-13.5Cr-1ThO$_2$ alloy, which appears to be slightly less recrystallized. In Figure 17b, c, and d it is seen that there are large dark inclusions (some appear as voids) extending to a depth

---

*In this phase of the report, the previous experimental creep data, structure description, particle parameters, etc., pertaining to the Ni-1% ThO$_2$ alloy will be included to facilitate comparisons with the three Cr-containing alloys.

TABLE 6. CHEMICAL ANALYSIS OF EXPERIMENTAL ALLOYS
FOR TRACE ELEMENTS

Element	Weight Percent			
	$Ni-1ThO_2$	$Ni-13.5Cr-1ThO_2$	$Ni-22.6Cr-1ThO_2$	$Ni-33.7Cr-1ThO_2$
Ti	<0.003	0.005	0.01	0.05
Ca	0.007	0.001	0.002	0.007
Al	0.003	0.1	0.3	0.3
Si	0.003	0.01	0.03	0.1
Mn	<0.003	0.02	0.02	0.05
Fe	0.02	0.1	0.1	0.1
Mg	<0.003	<0.003	<0.003	<0.003
Mo	--	0.01	0.01	0.01
Sn	--	0.003	<0.003	<0.003
Co	0.04	0.3	0.3	0.3
Ga	--	0.01	<0.005	<0.005
Cu	0.002	0.01	0.01	0.01
Ag	<0.001	<0.001	<0.001	<0.001
P	<0.003	--	--	--
S	0.002	--	--	--

TABLE 7. COMPOSITIONS AND ThO_2 PARTICLE SIZES AND SPACINGS OF
EXPERIMENTAL ALLOYS

Alloy	Analysis			Nominal Range of Particle Diameters, Å	Avg Particle Diameter, $2\bar{r}_v$, Å	Mean Planar Center-to-Center Particle Spacing[b] d, Å
	Wt % Cr	Wt % ThO_2	Vol % ThO_2			
Ni-1 ThO_2[a]	0	1.12	1.00	75-695	220	2505
Ni-13.5Cr-1 ThO_2	13.5	1.05	0.90	75-695	162	2070
Ni-22.6Cr-1 ThO_2	22.6	1.10	0.93	75-780	155	2165
Ni-33.7Cr-1 ThO_2	33.7	1.20	0.99	75-810	175	2290

(a) This is Alloy "A" from the preceding year's work [see Rept. No. NASA CR 54639, August 19, 1966; and References (7) and (8)].

(b) Calculated from Equation (1).
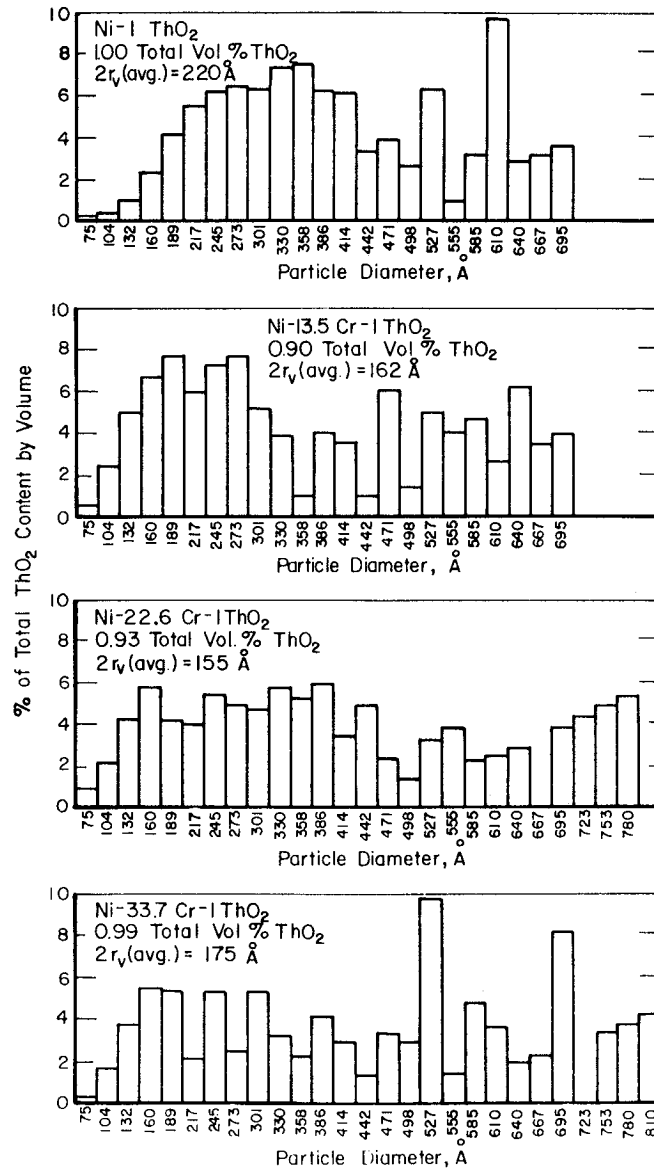
FIGURE 15. PARTICLE SIZE DISTRIBUTIONS OF EXPERIMENTAL ALLOYS, EXPRESSED AS VOLUME % OF TOTAL ThO$_2$ CONTENT
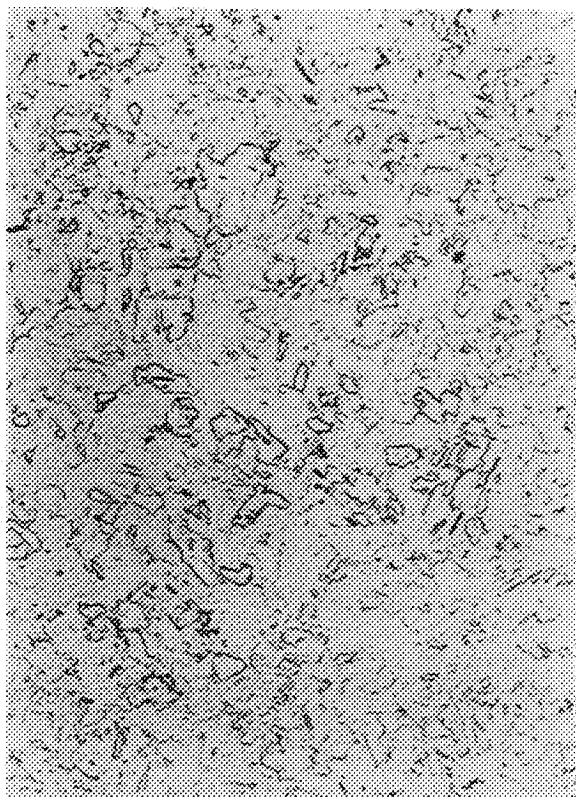
(a) Ni-1ThO$_2$
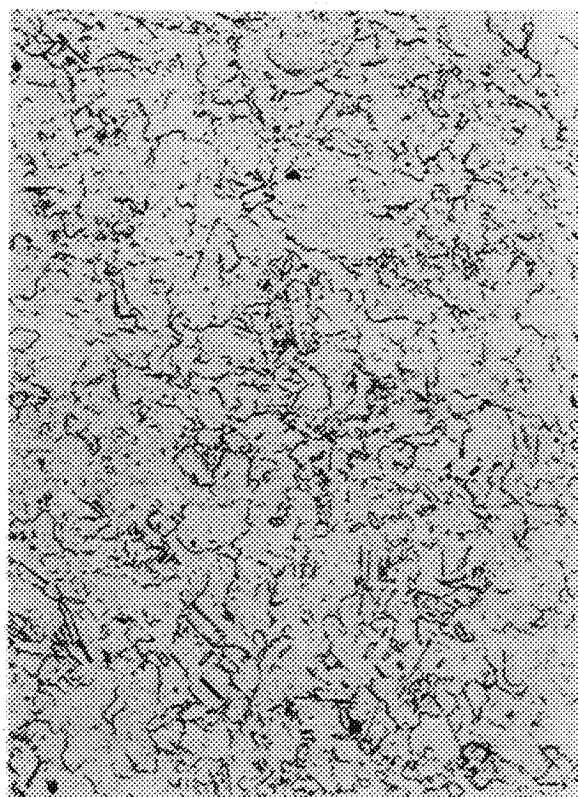
(b) Ni-13.5Cr-1ThO$_2$
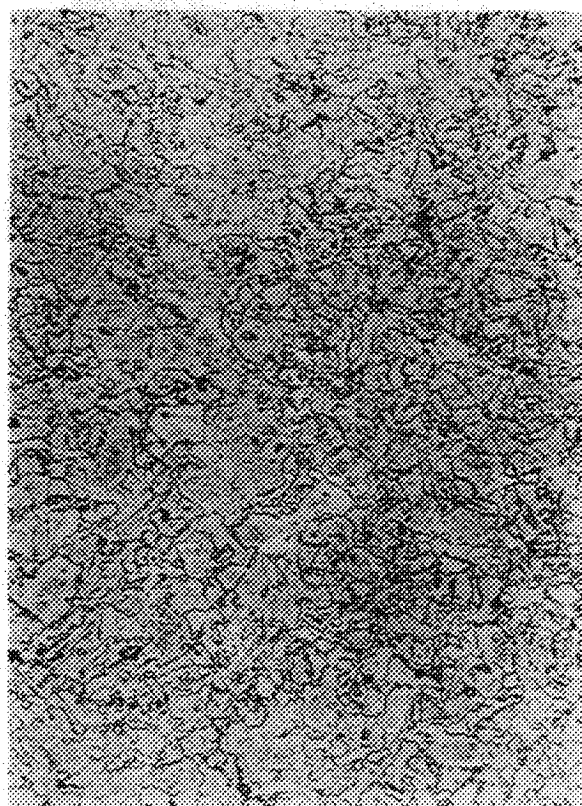
(c) Ni-22.6Cr-1ThO$_2$

(d) Ni-33.7Cr-1ThO$_2$

FIGURE 16. OPTICAL MICROGRAPHS OF AS-RECEIVED ALLOYS;
SHEET SURFACE, 100X
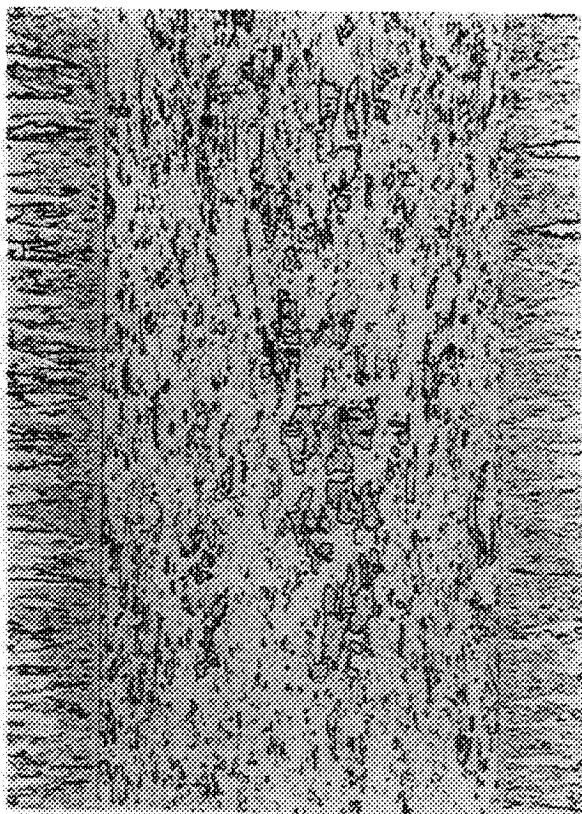
(a) Ni-1ThO$_2$
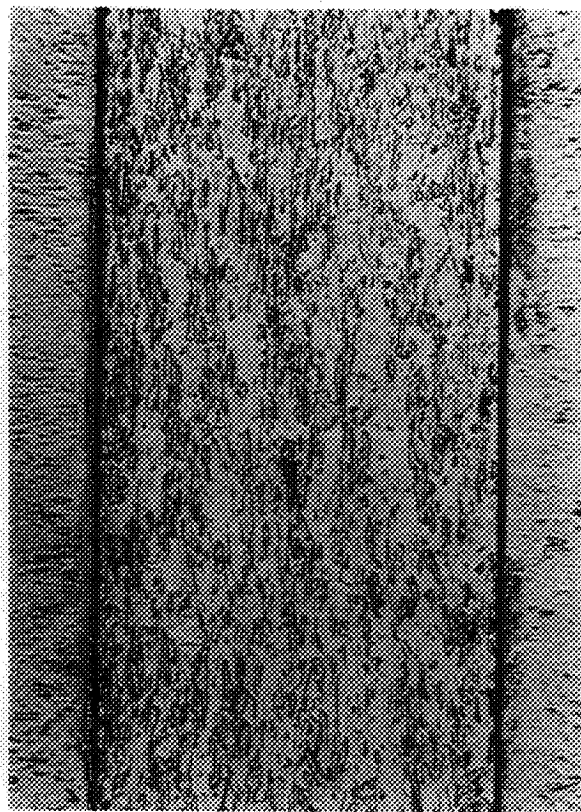
(b) Ni-13.5Cr-1ThO$_2$
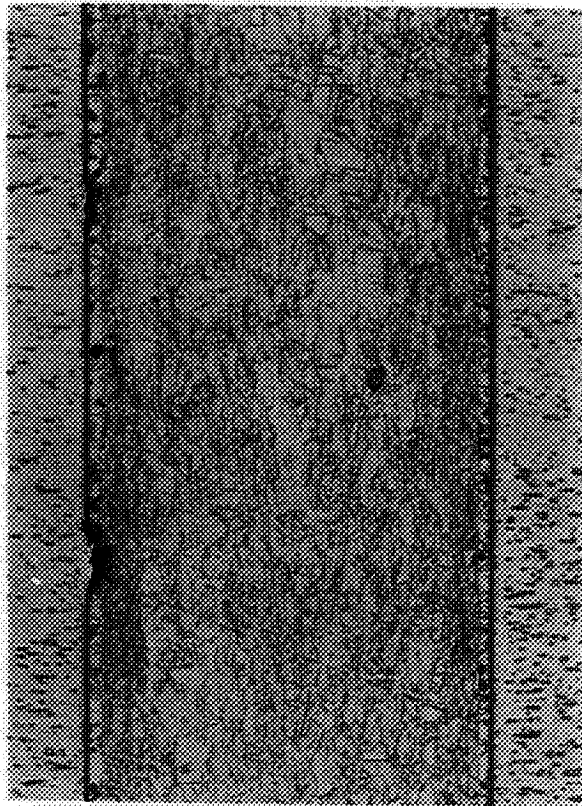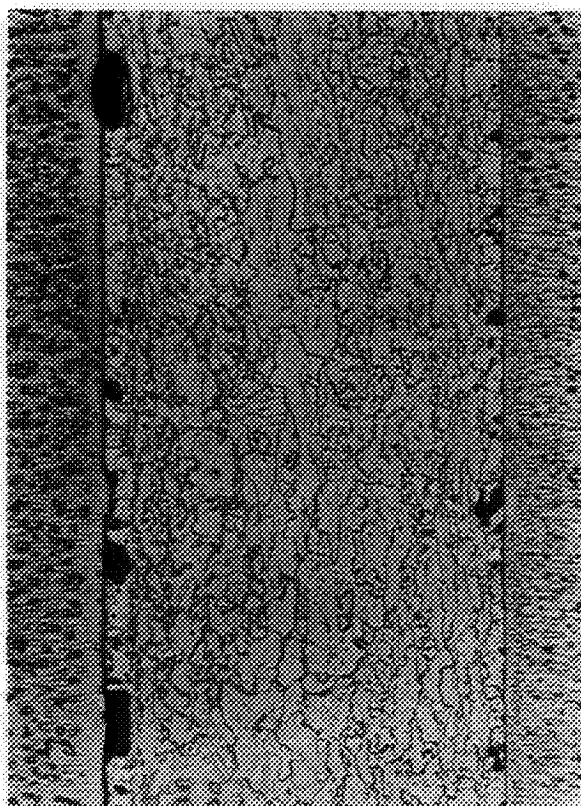
(c) Ni-22.6Cr-1ThO$_2$

(d) Ni-33.7Cr-1ThO$_2$

FIGURE 17. OPTICAL MICROGRAPHS OF AS-RECEIVED ALLOYS;
SHEET THICKNESS-NICKEL PLATED, 100X

(a) Ni-1ThO$_2$

(b) Ni-13.5Cr-1ThO$_2$

(c) Ni-22.6Cr-1ThO$_2$
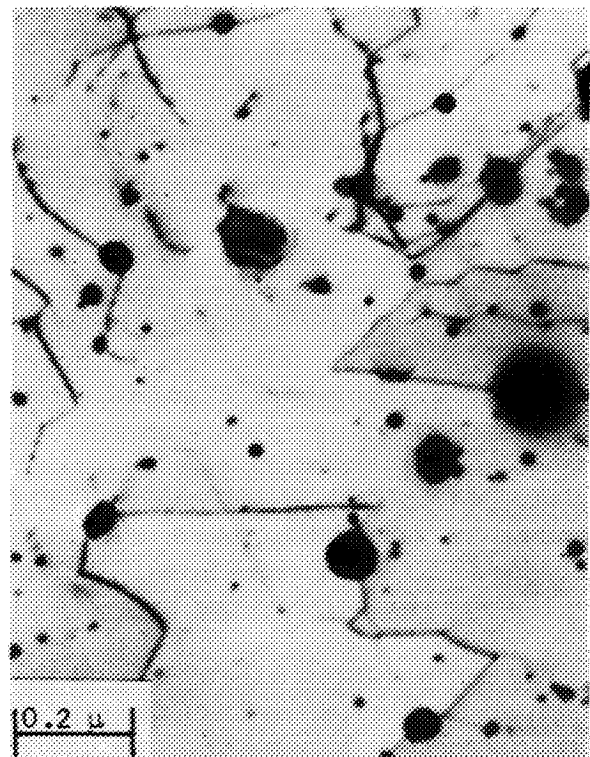
(d) Ni-33.7Cr-1ThO$_2$

FIGURE 18. TYPICAL TRANSMISSION ELECTRON MICROGRAPHS SHOWING THE
AS-RECEIVED STRUCTURE OF THE EXPERIMENTAL ALLOYS

of ~0.001 inch from the surface. These are probably Cr_2O_3 particles which became embedded during fabrication, and they are most prevalent in the 22.6% Cr and 33.7% Cr alloys. These inclusions were eliminated from the creep specimens by grinding 0.001-0.0015 inch from each surface of the three Cr-containing alloys.

The typical transmission electron micrographs in Figure 18 reveal that the four alloys have similar particle distributions and dislocation substructures. In each alloy the ThO_2 particles are quite uniformly dispersed and there is very little tendency for agglomeration. A dislocation substructure composed of regular networks is observed in many areas (see Figure 18a and b). Individual dislocations within the subgrains are strongly pinned by the ThO_2 particles, as noted in Figures 18c and d.

Based on the microstructural studies (Figures 16-18) and the comparable ThO_2 particle sizes and spacings (Table 7), it is concluded that the four alloys have the desired degree of initial structural uniformity.

RESULTS AND DISCUSSION

The Dependence of Steady-State Creep Rate on Temperature and Applied Stress

All creep data for the four alloys are listed in Table 8, and typical creep curves are illustrated in Figure 19 for the Ni-33.7Cr-1ThO_2 alloy tested at 925°C. These curves are similar in form to those of the other three alloys. In each case the total elongation at fracture was ~1 to 3%, and the fracture mode was predominately inter-granular, as seen in Figure 20. Fracture occurred by the growth and eventual merging of those grain boundary cracks nearly normal to the stress axis.

Crept specimens of the experimental alloys were examined by transmission elec-tron microscopy to determine how creep deformation influenced the dislocation structure. In many cases the general structural characteristics were essentially identical to those of uncrept specimens, although the creep deformation increased the dislocation density somewhat (e.g., compare Figure 21a with Figure 18c). In the alloy containing 33.7% Cr, the deformed structure often contained dislocations on a slip-band (see arrow at A in Figure 21b). This feature was observed only once in uncrept specimens. As in previous creep studies on "recrystallized" Ni-ThO_2 alloys[7, 8], there were dislocation-particle configurations which suggested that the ThO_2 particles were bypassed by climb, leaving "climb-jogs" on the dislocations. An example of this is shown in Figure 21b, point B, where the arrows point to the jogged dislocation and the particle that was bypassed.

The temperature dependence of the steady-state creep rate follows the usual Arrhenius relation for each of the four alloys (Figure 22), and the activation energies for creep are: Ni-1ThO_2, Q_c = 64 kcal/mole; Ni-13.5Cr-1ThO_2, Q_c = 65 kcal/mole; Ni-22.6Cr-1ThO_2, Q_c = 74 kcal/mole; Ni-33.7Cr-1ThO_2, Q_c = 78 kcal/mole. The activation energy for self-diffusion in Ni is 62-69 kcal/mole[40], and thus it is likely that creep of the Ni-1ThO_2 alloy is controlled by self-diffusion in the matrix. In fact it was suggested[7, 8] that the rate-controlling creep process for this alloy and other "recrystallized" Ni-ThO_2 alloys was the climb of edge dislocations over ThO_2 particles.

TABLE 8.   STEADY-STATE CREEP RATE OF Ni-Cr-1ThO$_2$
ALLOYS AS A FUNCTION OF TEMPERATURE
AND APPLIED STRESS

σ, psi	T, °C	$\dot{\epsilon}_s$, sec^{-1}	σ, psi	T, °C	$\dot{\epsilon}_s$, sec^{-1}
	Ni-1ThO$_2$			Ni-22.6Cr-1ThO$_2$	
7000	700	2.17×10^{-7}[a]	8000	900	6.55×10^{-7}
6000	725	2.17×10^{-7}[a]	8000	850	1.34×10^{-7}
5000	775	2.20×10^{-7}[a]	8000	825	6.53×10^{-8}
4000	875	7.12×10^{-7}[a]	8000	815	5.70×10^{-8}
4000	850	3.38×10^{-7}[a]	6500	900	2.86×10^{-7}
4000	825	2.33×10^{-7}[a]	5000	925	4.00×10^{-8}
4000	800	1.00×10^{-7}[a]	3500	1050	7.12×10^{-8}
3500	1050	1.47×10^{-5}	1965	1100	5.25×10^{-9}
2000	950	1.97×10^{-8}[a]	1670	1100	1.09×10^{-9}
1850	1100	1.05×10^{-7}		Ni-33.7Cr-1ThO$_2$	
1565	1100	2.90×10^{-8}	8000	900	1.07×10^{-7}
	Ni-13.5Cr-1ThO$_2$		8000	875	7.13×10^{-8}
7000	875	3.46×10^{-7}	8000	850	2.21×10^{-8}
7000	850	1.97×10^{-7}	8000	800	4.42×10^{-9}
7000	825	1.14×10^{-7}	7000	925	1.82×10^{-7}
7000	800	4.50×10^{-8}	6000	925	3.25×10^{-8}
6000	800	9.50×10^{-9}	4000	1025	6.40×10^{-8}
3500	1050	1.51×10^{-7}	3500	1050	4.36×10^{-8}
3000	1000	5.22×10^{-8}	2000	1100	1.89×10^{-9}
1930	1100	2.53×10^{-8}	1965	1100	2.01×10^{-8}
1640	1100	8.77×10^{-9}	1700	1100	6.27×10^{-10}

(a) These tests on the Ni-1ThO$_2$ alloy were reported previously [see Rept. No. NASA CR 54639, August 19, 1966, and Reference (8)].
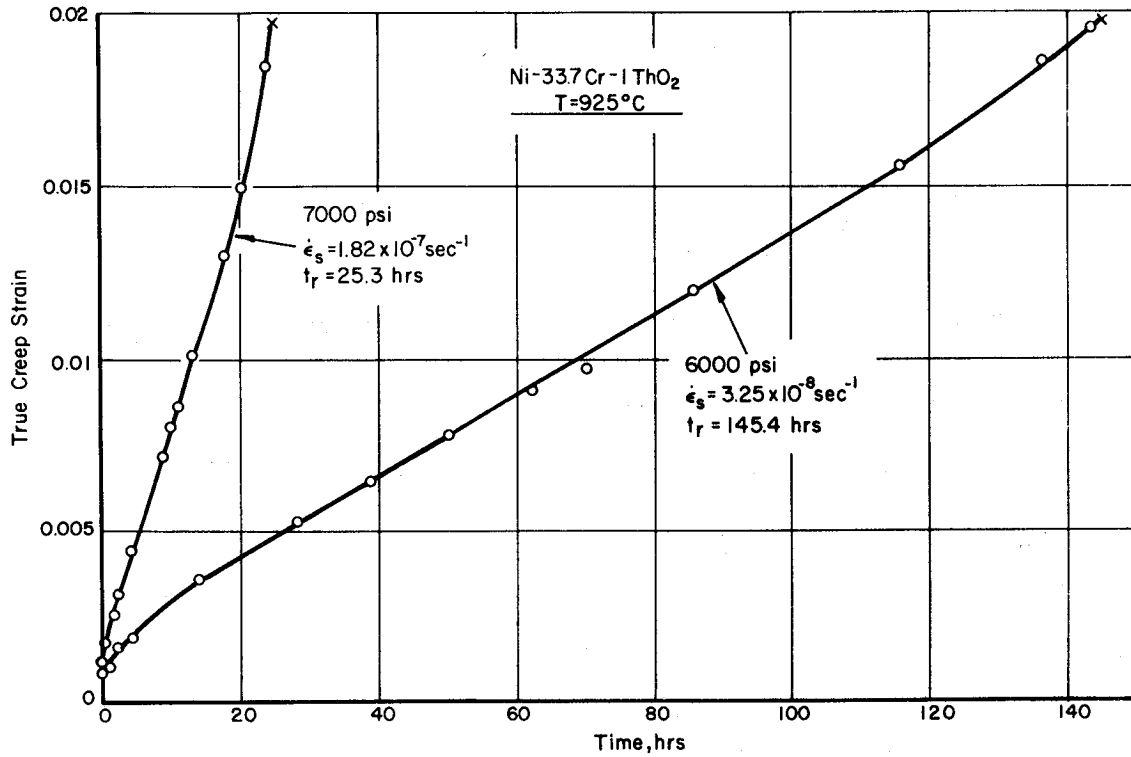
FIGURE 19. TYPICAL CREEP CURVES FOR THE EXPERIMENTAL
Ni-Cr-1ThO$_2$ ALLOYS

FIGURE 20. GRAIN BOUNDARY
CRACKS NEAR FRACTURE IN A
Ni-33.7Cr-1ThO$_2$ SPECIMEN CREPT
AT 8000 PSI AND 800°C; PLANE OF
SHEET, 600X

(a)   (b)
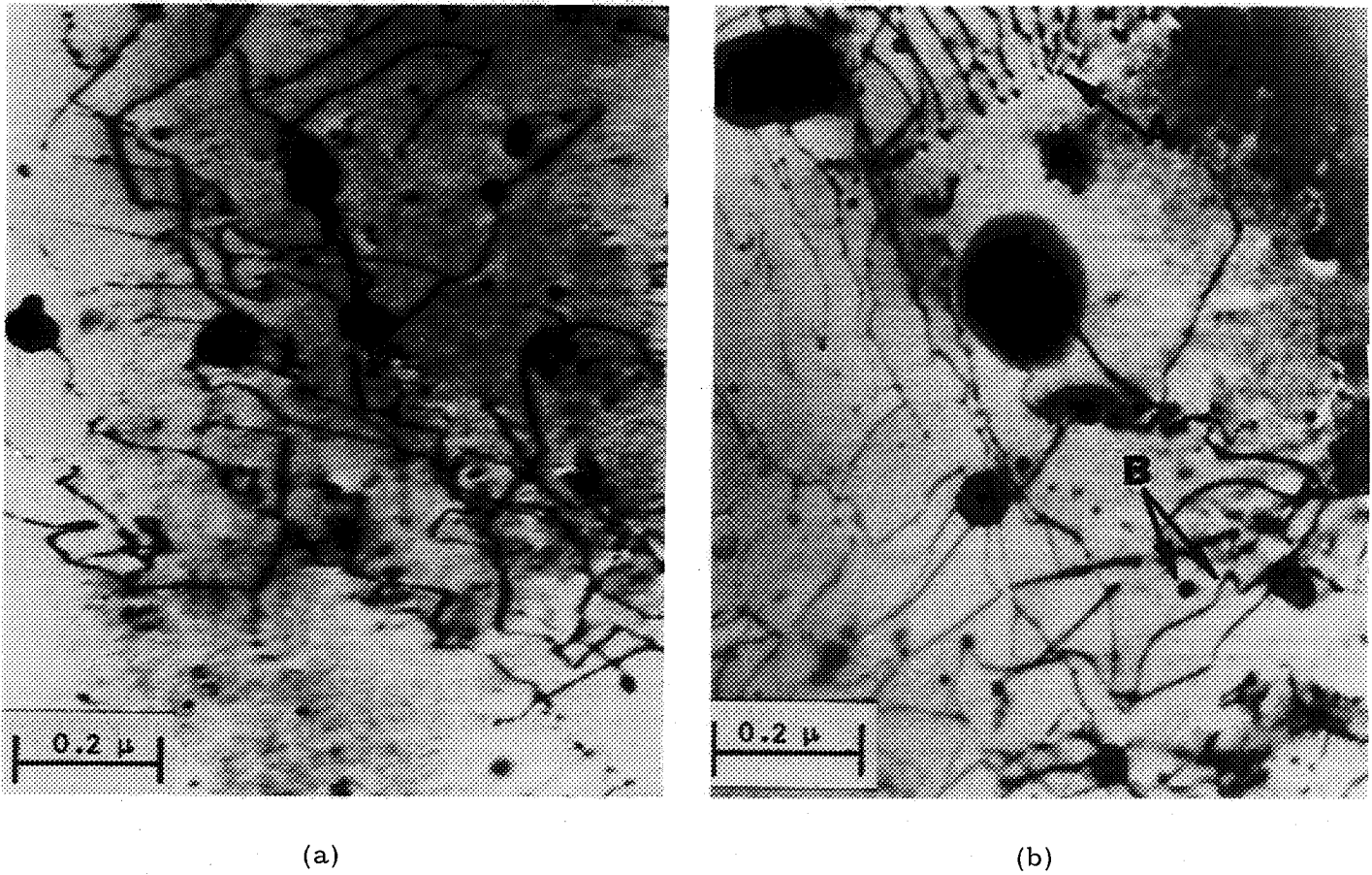
FIGURE 21. TYPICAL TRANSMISSION ELECTRON MICROGRAPHS
OF CREPT SPECIMENS

(a) Ni-22.6Cr-1ThO$_2$; σ = 8000 psi, T = 825°C,
3.0% total elongation.
(b) Ni-33.7Cr-1ThO$_2$; σ = 8000 psi, T = 850°C,
2.4% total elongation.
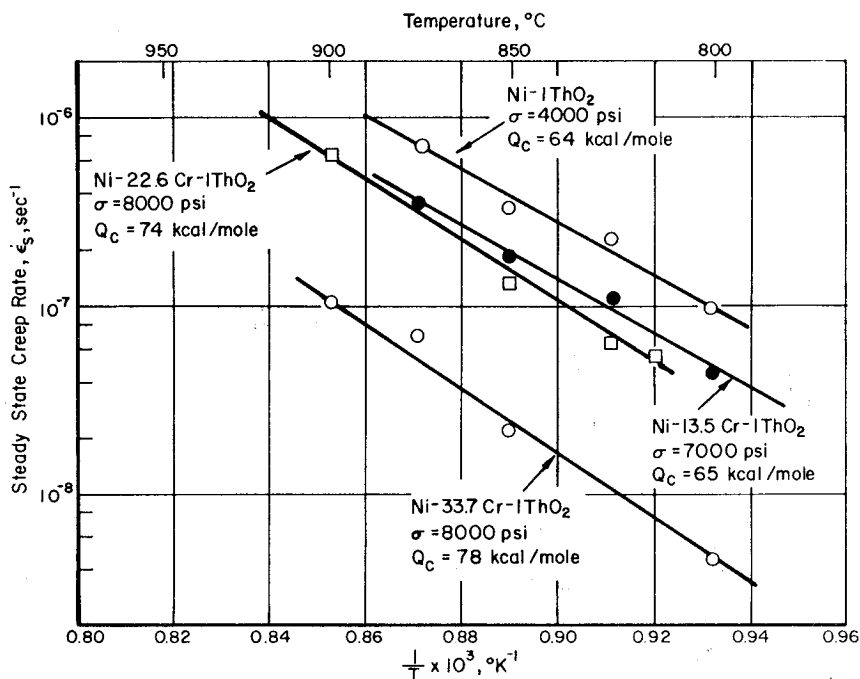
FIGURE 22. TEMPERATURE DEPENDENCE OF THE
STEADY-STATE CREEP RATE

There are no chemical self-diffusion activation energy data in the literature for
Ni-Cr alloys. Thus a direct comparison between Q_c and Q_{sd} in the Cr-containing alloys
is not possible. However, activation energies for intrinsic diffusion* of Ni and Cr in
Ni-Cr alloys are available[38,39], and these are plotted as a function of Cr content in
Figure 23. Here it is seen that the intrinsic diffusion activation energies are relatively
insensitive to composition, perhaps increasing slightly with increasing Cr content.
Also plotted in Figure 23 are creep activation energies as a function of Cr content for
the Ni-Cr-1ThO$_2$ alloys studied in this work and for binary Ni-Cr alloys[33,34]. Here
it is noted that Q_c increases from ~63-66 kcal/mole for 0% Cr to ~75-82 kcal/mole for
alloys containing 30% Cr. The absolute values of Q_c and the increase in Q_c with % Cr
are similar for the Ni-Cr-1ThO$_2$ alloys and the binary Ni-Cr alloys, which suggests
that the presence of 1% ThO$_2$ does not change the rate-controlling creep process.

It is assumed that the creep activation energies represent the chemical self-
diffusion activation energies in the respective alloys. This assumption is necessary, as
will be seen later, if the effect of stacking fault energy on creep is to be quantitatively
assessed using Equation (7). Equating Q_c to Q_{sd} for the Ni-Cr system is not unreason-
able, even though Q_c increases with % Cr more rapidly than do activation energies for
intrinsic diffusion (Figure 23). Chemical self-diffusion and intrinsic diffusion activation
energies in binary alloys do not always follow the same trend with composition[46].

The stress dependence of the temperature compensated creep rate is plotted in
Figure 24 for each of the four alloys. For reasons explained in the Appendix, the stress

*The terms "chemical diffusion" and "intrinsic diffusion" are discussed in the Appendix. Some authors[46] prefer the term
"interdiffusion" to "chemical diffusion".
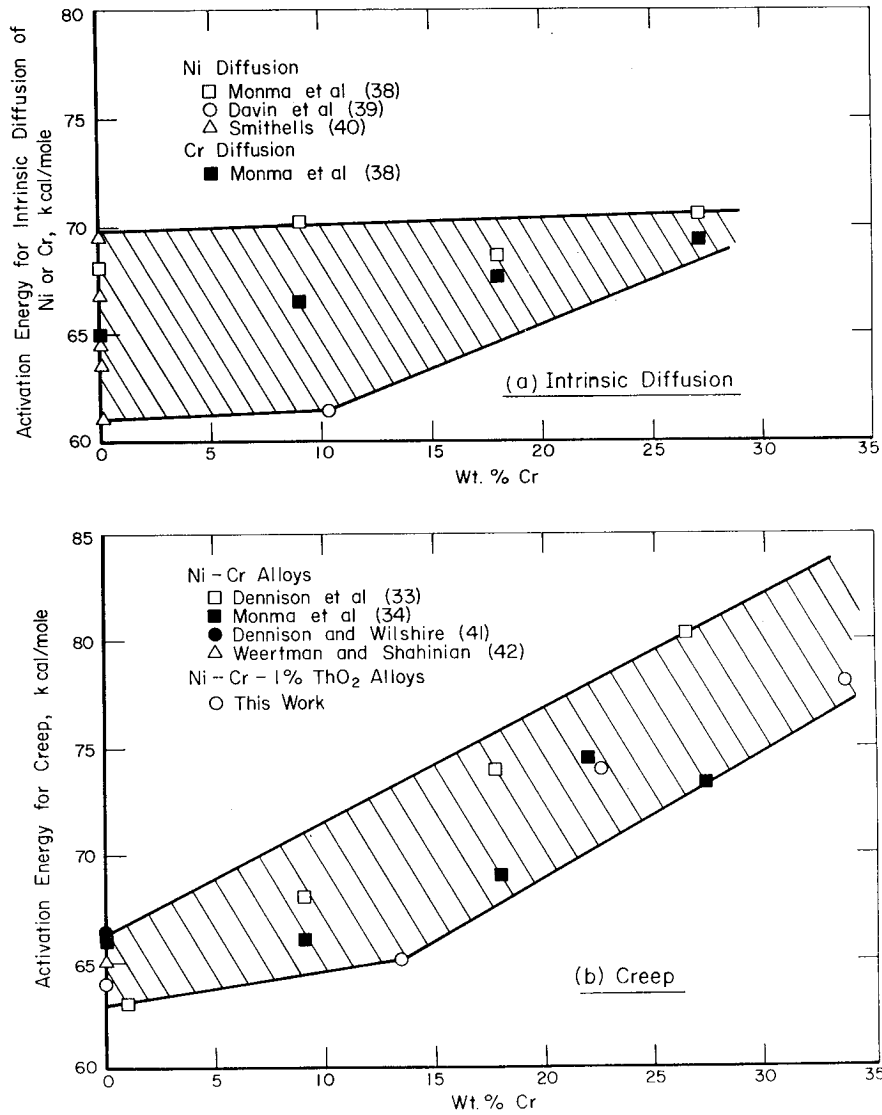
FIGURE 23. ACTIVATION ENERGIES FOR CREEP AND INTRINSIC DIFFUSION IN Ni-Cr AND Ni-Cr-1ThO$_2$ ALLOYS AS A FUNCTION OF COMPOSITION
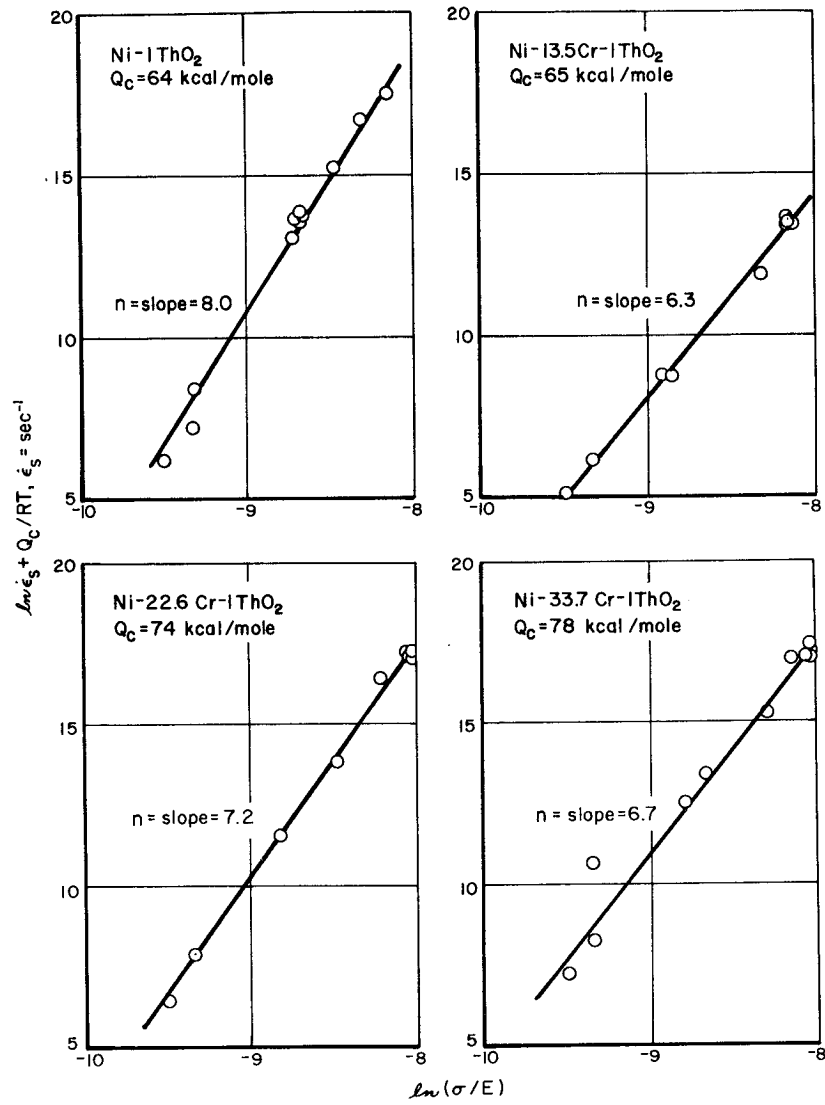
FIGURE 24. STRESS DEPENDENCE OF THE TEMPERATURE
COMPENSATED CREEP RATE

is plotted as (σ/E), where E is Young's modulus of a given alloy at the test temperature. From Figure 24 it is concluded that the activation energies for creep are stress independent over the range of stresses investigated. The stress dependence of the steady-state creep rate is of the form $\dot{\epsilon}_s \propto (\sigma/E)^n$, where n = 6.3-8.0, or n(avg) ≈ 7. These values of the stress exponent are somewhat higher than those observed in creep of binary Ni-Cr alloys by Monma, et al.[34] (n = 4.6-5.0). However, Dennison, et al.[33] found stress exponents of ~7 for creep of Ni-Cr alloys at 600°C. In this work, and in ThO_2-free Ni-Cr alloys[33,34] there was no systematic variation of the stress exponent with Cr content. The experimental creep results of the Ni-Cr-1ThO_2 alloys can thus be represented by the relation:

$$\dot{\epsilon}_s = C'(\sigma/E)^n \exp-(Q_c/RT) \quad . \tag{8}$$

It will be shown in the next section that the constant, C', contains the term γ^m, where γ is the stacking fault energy.

The Influence of Stacking Fault Energy on Steady-State Creep

At a given temperature and stress, increasing the Cr content in Ni-Cr-1ThO_2 and Ni-Cr alloys greatly decreases the creep rate. This is shown in Figure 25 where $\dot{\epsilon}_s$ is plotted versus wt % Cr for the alloys studied in this investigation and for binary Ni-Cr alloys studied by Monma, et al.[34] The decrease in $\dot{\epsilon}_s$ with increasing % Cr is not as rapid for Ni-Cr as for Ni-Cr-1ThO_2, but the general trend is the same. This is taken as further evidence that the presence of 1% ThO_2 does not change the rate-controlling creep process.

Figure 25 shows that for a given Cr composition, the ThO_2-containing alloys have creep rates ~10^2 times lower than binary Ni-Cr alloys, and this difference is somewhat larger at higher Cr contents. It appears, therefore, that the direct and indirect strengthening effects of ThO_2 in pure Ni are retained in the presence of Cr additions. Further creep strength improvement would be expected if the alloys had contained higher ThO_2 contents (say 2-3 vol %), and if optimum thermomechanical processing had been used to promote a stable, somewhat elongated, less recrystallized structure. This aspect will be discussed further in the next section.

It is reasonable to conclude that the decrease in steady-state creep rate with increasing % Cr is associated with a lowering of the stacking fault energy of the matrix. In order to quantitatively determine the effect of γ on $\dot{\epsilon}_s$ according to Equation (7), creep tests at constant (σ/E) were conducted at 1100°C for each of the four alloys. It was necessary to restrict these tests to 1100°C, since only at this temperature was it possible to calculate the chemical diffusivity, $\tilde{D}$, of each of the four alloys. $\tilde{D}$ was calculated from Darken's equation[44,45] using the intrinsic diffusivity data of Monma, et al.[38] and activity data reported by Hultgren, et al.[43] Details are given in the Appendix. Stacking fault energies of the matrix were taken from Figure A-3 (Appendix), and the relevant Young's Modulus values were obtained from data in the literature[48,49] and are plotted in Figures A-1 and A-2 (Appendix).

The pertinent diffusivity and stacking fault energy data are listed in Table 9 together with the steady-state creep rates determined at 1100°C for two values of σ/E.
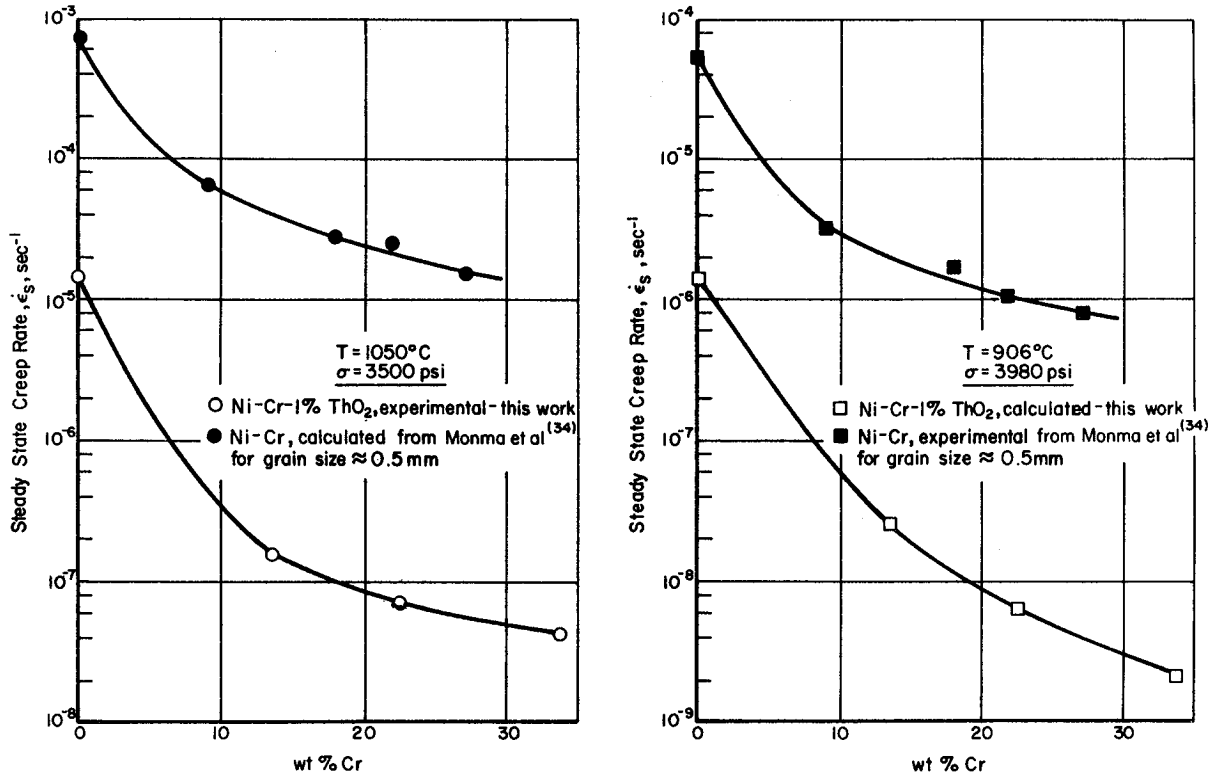
FIGURE 25. THE INFLUENCE OF Cr ON THE STEADY-STATE CREEP RATE OF
Ni-Cr-1ThO$_2$ AND Ni-Cr ALLOYS AT CONSTANT T AND σ

TABLE 9. DATA USED TO DETERMINE THE DEPENDENCE OF STEADY-STATE
CREEP RATE ON STACKING FAULT ENERGY

As Alloy	Room Temperature Matrix γ, erg/cm^2(a)	$\tilde{D}$ at 1100°C(b), cm^2/sec	σ/E(1100°C) = 8.90 x 10^{-5}		σ/E(1100°C) = 7.57 x 10^{-5}	
			$\dot{\epsilon}_s$, sec^{-1}	$\dot{\epsilon}_s/\tilde{D}$, cm^{-2}	$\dot{\epsilon}_s$, sec^{-1}	$\dot{\epsilon}_s/\tilde{D}$, cm^{-2}
Ni-1ThO$_2$	240	2.9 x 10^{-11}	1.05 x 10^{-7}	3.62 x 10^3	2.90 x 10^{-8}	1.00 x 10^3
Ni-13.5Cr-1ThO$_2$	140	5.6 x 10^{-11}	2.53 x 10^{-8}	4.52 x 10^2	8.77 x 10^{-9}	1.57 x 10^2
Ni-22.6Cr-1ThO$_2$	80	5.2 x 10^{-11}	5.25 x 10^{-9}	1.01 x 10^2	1.09 x 10^{-9}	2.10 x 10^1
Ni-33.7Cr-1ThO$_2$	60	3.8 x 10^{-11}	1.89 x 10^{-9}	4.97 x 10^1	6.27 x 10^{-10}	1.65 x 10^1

(a) Determined from data of Beeston and France[32] and Köster, et al.[31]; see Appendix , Figure A-3.
(b) Calculated from intrinsic diffusivity data of Monma, et al.[38], and activity data reported by Hultgren, et al.[43]; see Appendix.

The results are plotted in Figure 26 as log($\dot{\epsilon}_s/\tilde{D}$) versus log γ. From Figure 26, it is apparent that $\dot{\epsilon}_s \propto \gamma^m$, with m = 3.1-3.3. These values of the stacking fault energy exponent agree closely with the value of m = 3.5, determined by Sherby and co-workers[2,3] for pure FCC metals and α-brasses. Equations (7) and (8) can now be written as:

$$\dot{\epsilon}_s = C'' \gamma^m (\sigma/E)^n \exp-(Q_c/RT) \quad , \tag{9}$$

where $Q_c = Q_{sd}$. The creep parameters are summarized in Table 10.

A fundamental interpretation of the effects of γ on the steady-state creep rate is not straightforward. Based on these results and those of previous studies[2,3], it is probable that the creep process is self-diffusion controlled. Furthermore, it is reasonable to adopt a dislocation-climb process as being rate-controlling. For example, previous experimental evidence[7,8] on recrystallized Ni-ThO$_2$ alloys (including the Ni-1ThO$_2$ alloy discussed here) pointed strongly toward climb of edge dislocations as being the rate-determining creep process.

However, it is not exactly clear how the dislocation width influences the climb process. Weertman[36] assumed that core diffusion down perfect dislocations (high γ) was more rapid than down widely split dislocations (low γ). This predicted a lower dislocation climb rate with decreasing γ, which in turn would result in a slower creep rate. As noted earlier, the dislocation core diffusion measurements of Birnbaum, et al.[37] indicate that Weertman's original assumption may be incorrect. This does not mean, however, that the final predictions of Weertman's theory are wrong, i.e., the average climb rate may decrease with decreasing γ.

One way of approaching this problem, which might lead to a formulation that predicts a decreased climb rate with decreasing γ, is as follows. As the width of a dislocation increases, it is more difficult to form jogs on the dislocation, and the average jog density per dislocation line would be lower for lower γ alloys. If the vacancies associated with the process of dislocation climb are created or destroyed at jogs[36], then the lower jog density would lower the average climb rate.
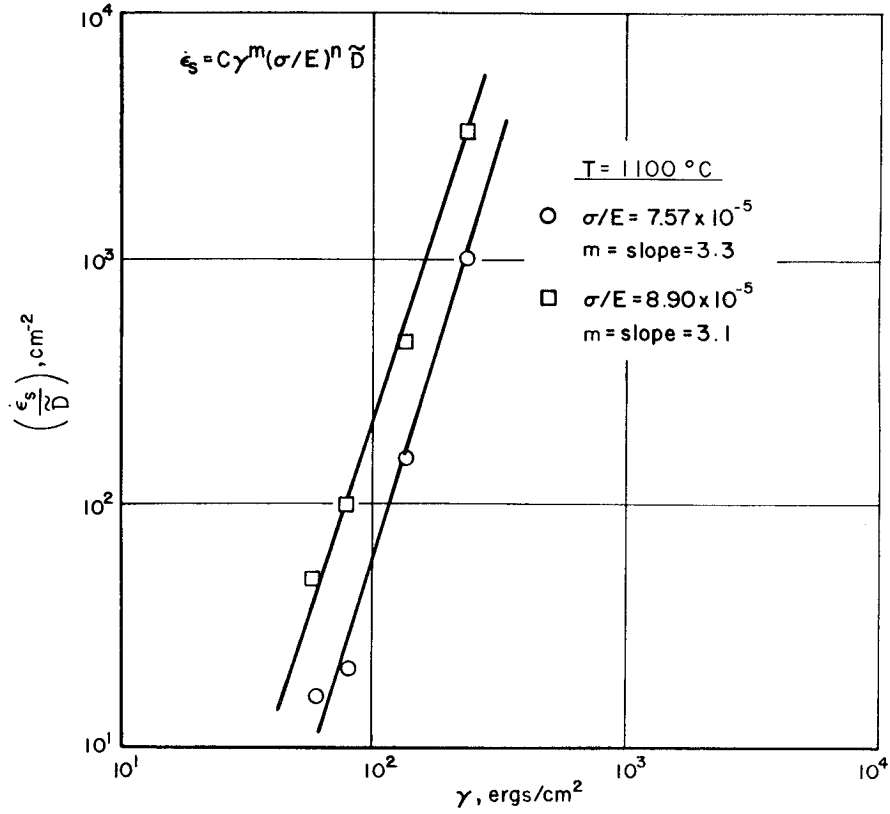
FIGURE 26. LOG-LOG PLOT OF DIFFUSIVITY COMPENSATED STEADY-STATE CREEP RATE AS A FUNCTION OF STACKING FAULT ENERGY

TABLE 10. SUMMARY OF CREEP PARAMETERS FOR Ni-Cr-1ThO$_2$ ALLOYS

Alloy	Q$_c$, kcal/mole	n	m
Ni-1ThO$_2$	64	8.0	3.1-3.3
Ni-13.5Cr-1ThO$_2$	65	6.3	3.1-3.3
Ni-22.6Cr-1ThO$_2$	74	7.2	3.1-3.3
Ni-33.7Cr-1ThO$_2$	78	6.7	3.1-3.3

More specifically, consider that dislocations are impeded during creep by obstacles such as ThO$_2$ particles. A dislocation intersecting an array of particles will bow between the particles and might bypass the particles by climb, cross-slip, Orowan-bowing, shearing the particles, etc. Suppose that the bypass mechanism is climb over the particles. The dislocation is constricted over a short length where it is pressed against the particle[1], which would in turn cause a local increase in the jog density. The constricted segment pinned at the particle then would climb at a higher rate than the rest of the dislocation line until eventually the particle was bypassed. The wider the dislocation is split (i.e., the lower the stacking fault energy) the more difficult it is to constrict. It would thus be easier for a narrow dislocation to accomplish the climb event than for a widely split one. This concept, as yet, has not been sufficiently examined to allow formulation of a climb model incorporating the effects of stacking fault energy on the dislocation climb rate.

Comparison of Creep Behavior of the Experimental Ni-22.6Cr-1ThO$_2$ Alloy With a Commercial Ni-20Cr-2ThO$_2$ Alloy (TD NiC) and a Binary Ni-22Cr Alloy

In a previous communication[9], the authors presented results on the high temperature creep behavior of TD NiC sheet. This material contained 21.3 wt % Cr and 2.2 vol % ThO$_2$. The average ThO$_2$ particle diameter was 145 Å and the mean planar center-to-center particle spacing was calculated to be 1320 Å from Equation (1). Most of the creep tests were performed in air, but several vacuum tests were made for comparison purposes. Also specimens were tested such that their axes were either parallel or transverse to the primary sheet rolling direction.

It is instructive to compare the steady-state creep rate of TD NiC sheet at a given temperature and stress with those of the Ni-22.6Cr-1ThO$_2$ alloy studied in this work and a Ni-22Cr alloy tested by Monma, et al.[34] This comparison is made in Table 11, where it is seen that the TD NiC sheet has the lowest creep rate, and the binary Ni-22Cr alloy has the highest value of $\dot{\epsilon}_s$. The very high $\dot{\epsilon}_s$ value calculated for the Ni-22Cr alloy is artificial and indicates that this alloy would fail on loading at this stress and temperature. It is evident, however, that the presence of ThO$_2$ particles drastically lowers the steady-state creep rate, the effect being magnified the higher the ThO$_2$ content. It should be obvious from previous discussions, that the creep strengthening influence of ThO$_2$ particles is twofold: (1) direct strength improvement due to particles blocking dislocation motion during creep and (2) indirect strengthening arising from the

fact that the particles serve to stabilize a fine grain and subgrain structure during fabrication. In fact the thermomechanical processing used to make TD NiC sheet is purposely designed to take advantage of this indirect strengthening concept.

TABLE 11. A COMPARISON OF THE CREEP RATE OF TD NiC SHEET, Ni-22.6Cr-1ThO$_2$ AND Ni-22Cr at T = 927°C and σ = 14,000 psi

| Alloy | ThO$_2$ Particle Parameters | | Structure | $\dot{\epsilon}_s$, sec^{-1} | Reference |
	Avg Diam., $2r_v$, Å	Spacing, d, Å			
Ni-22Cr	--	--	Recrystallized, g.s. = 0.5 mm	5.03 x 10$^{2(a)}$	(34)
Ni-22.6Cr-0.93 vol % ThO$_2$	155	2165	"Recrystallized" See Figure 16-18	1.01 x 10$^{-4(b)}$	(This work)
Ni-21.3Cr-2.2 vol % ThO$_2$ (TD NiC)	145	1320	Partially recry-stallized, grains somewhat elon-gated in rolling direction	1.89 x 10$^{-8(c)}$	(9)

(a) Calculated from Reference (34).
(b) Calculated from Figure 24.
(c) Experimental data, for a vacuum creep test, where the specimen axis was parallel to the primary sheet rolling direction.

ACKNOWLEDGMENTS

REFERENCES

(1) B. A. Wilcox and A. H. Clauer, "Creep of Thoriated Nickel Above and Below 0.5 T_m", Trans. AIME, 236, 570 (1966).

(2) C. R. Barrett and O. D. Sherby, "Influence of Stacking Fault Energy on High-Temperature Creep of Pure Metals", Trans. AIME, 233, 1116 (1965).

(3) R. M. Bonesteel and O. D. Sherby, "Influence of Diffusivity, Elastic Modulus, and Stacking Fault Energy on the High-Temperature Creep Behavior of Alpha Brasses", Acta Met., 14, 385 (1966).

(4) B. A. Wilcox and R. I. Jaffee, "Direct and Indirect Strengthening Effects of ThO_2 Particles in Dispersion-Hardened Nickel", paper presented at International Conference on Strength of Metals and Alloys, Tokyo, September 4-8, 1967 (to be published by Japan Inst. Met.).

(5) N. J. Grant and O. Preston, "Dispersed Hard Particle Strengthening of Metals", Trans. AIME, 209, 349 (1957).

(6) G. S. Ansell, "The Mechanism of Dispersion-Strengthening: A Review", paper presented at Oxide Dispersion Strengthening Conference, Bolton Landing, New York, June 27-29, 1966 (to be published by Gordon and Breach).

(7) B. A. Wilcox and A. H. Clauer, "High Temperature Creep of Ni-ThO_2 Alloys", ibid.

(8) A. H. Clauer and B. A. Wilcox, "Steady-State Creep of Dispersion-Strengthened Nickel", Met. Sci. J., 1, 86 (1967).

(9) B. A. Wilcox, A. H. Clauer, and W. S. McCain, "Creep and Creep Fracture of a Ni-20Cr-2ThO_2 Alloy", Trans. AIME, 239, 1791 (1967).

(10) V. A. Tracey and D. K. Worn, "Some Observations on the Cold-Drawing and Annealing Behavior of Nickel Containing a Dispersed Phase of Thoria", Powder Met., No. 10, 34 (1962).

(11) G. S. Doble and R. J. Quigg, "Effect of Deformation on the Strength and Stability of TD Nickel", Trans. AIME, 233, 410 (1965).

(12) J. E. White and R. D. Carnahan, "A Microplasticity Study of Dispersion Strengthening in TD Nickel", Trans. AIME, 230, 1298 (1964).

(13) M. von Heimendahl and G. Thomas, "Substructure and Mechanical Properties of TD Nickel", Trans. AIME, 230, 1520 (1964).

(14) R. W. Fraser and D. J. I. Evans, "The Strengthening Mechanism in Dispersion Strengthened Nickel", paper presented at Oxide Dispersion Strengthening Conference, Bolton Landing, New York, June 27-29, 1966 (to be published by Gordon and Breach).

(15) G. S. Doble, L. Leonard, and L. J. Ebert, "The Effect of Deformation on Dispersion Hardened Alloys", Final Rept. on NASA Grant NGR 36-033-094, November, 1967.

(16) R. L. Fullman, R. P. Carreker, and J. C. Fisher, "Simple Devices for Approximating Constant Stress During Tensile Creep Tests", Trans. AIME, 197, 657 (1953).

(17) B. A. Wilcox and A. H. Clauer, "Creep Fracture of Thoriated Nickel", Trans. AIME, 233, 253 (1965).

(18) M. F. Ashby, "The Hardening of Metals by Non-Deforming Particles", Z. für Metallk., 55, 5 (1964).

(19) M. F. Ashby, "A Theory of the Critical Shear Stress and Work Hardening in Dispersion Hardened Crystals", paper presented at Oxide Dispersion Strengthening Conference, Bolton Landing, New York, June 27-29, 1966 (to be published by Gordon and Breach).

(20) D. Killpatrick, A. Phillips, and V. Kerlins, "Fracture in Dispersion Strengthened Nickel-Chromium Alloys", Douglas MSSD Report, DAC 59579, August 24, 1967.

(21) D. Webster, Boeing Commercial Airplane Division, Seattle, private communication.

(22) W. D. Jenkins, T. G. Digges, and C. R. Johnson, "Tensile Properties of Copper, Nickel, and 70-Percent-Copper-30-Percent-Nickel and 30-Percent-Copper-70-Percent-Nickel Alloys at High Temperatures", J. Res. Nat. Bur. Std., 58, 201 (1957).

(23) E. Macherauch and O. Vöhringer, "The Deformation Behavior of Polycrystalline Nickel", Phys. Stat. Sol., 6, 491 (1964).

(24) R. W. Fraser, Sherritt Gordon Mines, Ltd., Fort Saskatchewan, Alberta, Canada, unpublished data.

(25) International Nickel Co., Sterling Forest, New York, unpublished data.

(26) M. G. Lozinsky and N. Z. Pertsovsky, "The Peculiarities of the Deformation of Nickel at Various Temperatures and Strain Rates", Izvest. Akad. Nauk S.S.S.R., 4, 90 (1962).

(27) R. E. Stuart and C. D. Starr, "New Design Data on TD Nickel", Mat. Design Engr., 58, 81 (1963).

(28) J. F. Wygant, "Elastic and Flow Properties of Dense, Pure Oxide Refractories", J. Am. Ceram. Soc., 34, 374 (1951).

(29) C. Susse, "Measurement of the Shear Modulus of Nickel up to 1000°C", J. Phys. Radium, 17, 910 (1956).

(30) P. Haasen, "Plastic Deformation of Nickel Single Crystals at Low Temperatures", Phil. Mag., 3, 384 (1958).

(31) E. H. Köster, A. R. Thölén, and A. Howie, "Stacking Fault Energies of Ni-Co-Cr Alloys", Phil. Mag., 10, 1093 (1964).

(32) B. E. P. Beeston and L. K. France, "The Stacking Fault Energies of Some Binary Nickel Alloys Fundamental to the Nimonic Series", to be published in Met. Sci. J. (Inst. of Met., London).

(33) J. P. Dennison, R. J. Llewllyn, and B. Wilshire, "The Creep and Fracture Properties of Some Nickel-Chromium Alloys at 600°C", J. Inst. Met., 95, 115 (1967).

(34) K. Monma, H. Suto, and H. Oikawa, "High Temperature Creep of Nickel-Chromium Alloys", J. Japan Inst. Met., 28, 253 (1964).

(35) C. K. L. Davies, P. W. Davies, and B. Wilshire, "The Effect of Variations in Stacking-Fault Energy on the Creep of Nickel-Cobalt Alloys", Phil. Mag., 12, 827 (1965).

(36) J. Weertman, "Theory of the Influence of Stacking-Fault Width of Split Dislocations on High-Temperature Creep Rate", Trans. AIME, 233, 2069 (1965).

(37) H. K. Birnbaum, M. Wuttig, and C. Baker, "Self-Diffusion Along Dislocation Lines; The Effect of Stacking Fault Energy", paper presented at International Conference on Strength of Metals and Alloys, Tokyo, September 4-8, 1967 (to be published by Japan Inst. Met.).

(38) K. Monma, H. Suto, and H. Oikawa, "Diffusion of Ni^{63} and Cr^{51} in Nickel-Chromium Alloys", J. Japan Inst. Met., 28, 188 (1964).

(39) A. Davin, V. Leroy, D. Coutsouradis, and L. Habraken, "Comparison of the Diffusion of Some Substitution Elements in Nickel and Cobalt", Cobalt, No. 19, 51 (June, 1963).

(40) C. J. Smithells, Metals Reference Book, 3rd Ed., Vol 2, Butterworth, Washington, D. C. (1962), p 595.

(41) J. P. Dennison and B. Wilshire, "Observations on the Influence of Impurities on the Creep and Fracture Behavior of Nickel at 500 and 600°C", J. Inst. Met., 91, 343 (1962-63).

(42) J. Weertman and P. Shahinian, "Creep of Polycrystalline Nickel", Trans. AIME, 206, 1223 (1956).

(43) R. Hultgren, R. L. Orr, P. D. Anderson, and K. K. Kelly, Selected Values of Thermodynamic Properties of Metals and Alloys, Wiley, New York (1963), p 663.

(44) L. S. Darken and R. W. Gurrey, Physical Chemistry of Metals, McGraw-Hill, New York (1953), p 463.

(45) P. G. Shewmon, Diffusion in Solids, McGraw-Hill, New York (1963), p 126.

(46) J. E. Reynolds, B. L. Averbach, and M. Cohen, "Self-Diffusion and Interdiffusion in Gold-Nickel Alloys", Acta Met., 5, 29 (1957).

(47)   D. McLean and K. F. Hale, <u>Structural Processes in Creep</u>, Iron and Steel Inst.,
London (1961), p 19.

(48)   J. L. Lytton, J. A. Hren, K. T. Kamber, and O. D. Sherby, "Apparatus for the
Determination of Dynamic Young's Modulus and Internal Friction in Vacuum at
Temperatures From 25°C to 1200°C", Brit. J. Appl. Phys., 14, 1573 (1964).

(49)   T. Ya. Benieva and I. G. Polotsky, "Influence of Certain Factors on the Elastic
Properties of Nickel and Nickel-Chromium-Base Alloys", Fiz. Metallov i Metal-
lovedenie, 12, 584 (1961).

(50)   I. L. Dillamore, R. E. Smallman, and W. T. Roberts, "A Determination of the
Stacking-Fault Energy of Some Pure F.C.C. Metals", Phil. Mag., 9, 517 (1964).

(51)   M. J. Whelan, "Dislocation Interactions in F.C.C. Metals, With Particular
Reference to Stainless Steel", Proc. Roy. Soc. A, 249, 114 (1959).

(52)   H. J. McQueen, W. A. Wong, and J. J. Jonas, "Deformation of Aluminum at
High Temperatures and Strain Rates", Canadian J. Phys., 45, 1225 (1967).

APPENDIX

PERTINENT DATA AND CALCULATIONS CONCERNING CHEMICAL
DIFFUSIVITIES, ELASTIC MODULI, AND STACKING FAULT ENERGIES

APPENDIX

PERTINENT DATA AND CALCULATIONS CONCERNING CHEMICAL DIFFUSIVITIES, ELASTIC MODULI, AND STACKING FAULT ENERGIES

Chemical Diffusivity

The equation used to treat the creep data of the Ni-Cr-1ThO$_2$ alloys is:

$$\dot{\epsilon}_s = C\gamma^m \, (\sigma/E)^n \, \tilde{D} \quad , \tag{A-1}$$

where $\dot{\epsilon}_s$ = steady-state creep rate, C = constant, γ = stacking fault energy of the matrix, σ = applied stress, E = Young's modulus of a particular alloy at the test temperature, and $\tilde{D}$ = the matrix chemical self-diffusivity of a given alloy at the test temperature. In order to examine accurately only the influence of γ on $\dot{\epsilon}_s$ it is necessary to make the modulus correction[2] and to know the chemical self-diffusivity, $\tilde{D}$, of the various alloys at the test temperatures. The stacking fault energy exponent, m, can then be determined by plotting log $(\dot{\epsilon}_s/\tilde{D})$ versus log γ, for constant values of σ/E.

If the rate controlling creep process (e. g., dislocation climb) is self-diffusion controlled, then the activation energy for creep, Q_c, should equal the activation energy for self-diffusion, Q_{sd}, since $\tilde{D} = \tilde{D}_o \exp-(Q_{sd}/RT)$.

The term "chemical diffusivity" can be thought of as a measure of how fast vacancies move in a binary alloy (such as Ni-Cr), and it is related to the mobility of both diffusing species in that alloy. $\tilde{D}$ is usually determined by a Boltzmann-Matano analysis of diffusion couples. An extensive review of the literature revealed that no chemical diffusivity data existed for the Ni-Cr system. However, it is possible to calculate $\tilde{D}$ for binary alloys provided the appropriate thermodynamic data are available. This can be done using Darken's equation[44, 45]:

$$\tilde{D} = \left(D_1^* N_2 + D_2^* N_1 \right) \left(1 + \frac{d\ell n \, \gamma_1}{d\ell n \, N_1} \right) \quad . \tag{A-2}$$

Here D_1^* and D_2^* are the intrinsic diffusivities of components 1 and 2 in a given binary alloy (determined by radioactive tracer experiments), N_1 and N_2 are the mole fractions, and γ_1 is the activity coefficient of component 1.

In the Ni-Cr system the only available activity coefficient data are at T = 1100°C [reported by Hultgren, et al.[43]]. Using this information and the intrinsic diffusivity data of Monma, et al.[38], the $\tilde{D}$ (1100°C) values for each experimental alloy were calculated and are listed in Table A-1. It is noted that a maximum value of $\tilde{D}$ is found for the alloy containing 13.5% Cr. This behavior has also been experimentally observed in the Au-Ni system at the Ni-rich end[46].

Since the chemical diffusivities could be calculated at only 1100°C, it was necessary to perform creep experiments for each alloy at that temperature in order to evaluate the stacking fault energy exponent, m.

TABLE A-1. RESULTS OF CHEMICAL DIFFUSIVITY CALCULATIONS FOR
Ni-Cr ALLOYS AT 1100°C, USING DARKEN'S RELATION

Alloy[a]	Intrinsic Diffusivities[38]		Calculated Chemical Diffusivity, $\tilde{D}$, cm^2/sec
	D^*_{Ni}, cm^2/sec	D^*_{Cr}, cm^2/sec	
Ni	2.9×10^{-11}	--	2.9×10^{-11}
Ni-13.5 wt% Cr	2.6×10^{-11}	3.4×10^{-11}	5.6×10^{-11}
Ni-22.6 wt% Cr	2.1×10^{-11}	3.2×10^{-11}	5.2×10^{-11}
Ni-33.7 wt% Cr	1.95×10^{-11}	3.0×10^{-11}	3.8×10^{-11}

(a) In these calculations it was considered that the presence of 1% ThO_2 was negligible, and that the $\tilde{D}$ values for binary Ni-Cr alloys were appropriate to the respective ThO_2-containing Ni-Cr alloys.

Elastic Moduli

When plotting creep data for a given pure metal or alloy it is often not necessary to correct the stress term for the elastic modulus, which is temperature dependent. That is, the expression $\dot{\epsilon}_s \propto \sigma^n$ would give about the same exponent, n, as the relation $\dot{\epsilon}_s \propto (\sigma/E)^n$. This happens because the range of test temperatures is frequently small enough so that there is not a significant variation in E over that temperature range. However, when the stress dependence of $\dot{\epsilon}_s$ for various pure metals and alloys are compared, it is more appropriate to normalize the stress term by expressing it as (σ/E).[2, 47] This convention is particularly necessary if alloys are being compared to assess the influence of stacking fault energy on $\dot{\epsilon}_s$.

Thus, the present creep results on Ni-Cr-1ThO_2 alloys were treated in this manner. In each case the isotropic, polycrystalline, unrelaxed elastic modulus was used. Figure A-1 is a plot of Young's modulus versus temperature for pure Ni[48] and two alloys: Ni-9.4 wt % Cr and Ni-21.4 wt % Cr.[49] The temperature dependence of the shear modulus of Ni is also included in Figure A-1. At ~700-800°C, the dynamic elastic moduli drop sharply with increasing temperature because of processes such as grain boundary relaxation. Thus, to obtain high temperature unrelaxed modulus values, the extrapolated dashed lines were used. In Figure A-2 the unrelaxed Young's modulus at 1100°C is plotted as a function of Cr content. This curve was used to determine E (1100°C) for the four experimental alloys.

Stacking Fault Energies

As Cr is added to Ni there is a marked decrease in the room temperature stacking fault energy, γ. In order to correlate high temperature creep data with room temperature stacking fault energy, it is necessary (and customary) to assume that γ is relatively temperature independent. The most complete data in the Ni-Cr system is that due to Beeston and France[32] who used the rolling texture method of stacking fault energy measurement[50]. However, it is noted in Figure A-3 that an independent measurement at 30% Cr by Köster, et al.[31] agrees well with the data of Beeston and France. Köster, et al. used transmission electron microscopy to measure radii of curvature of
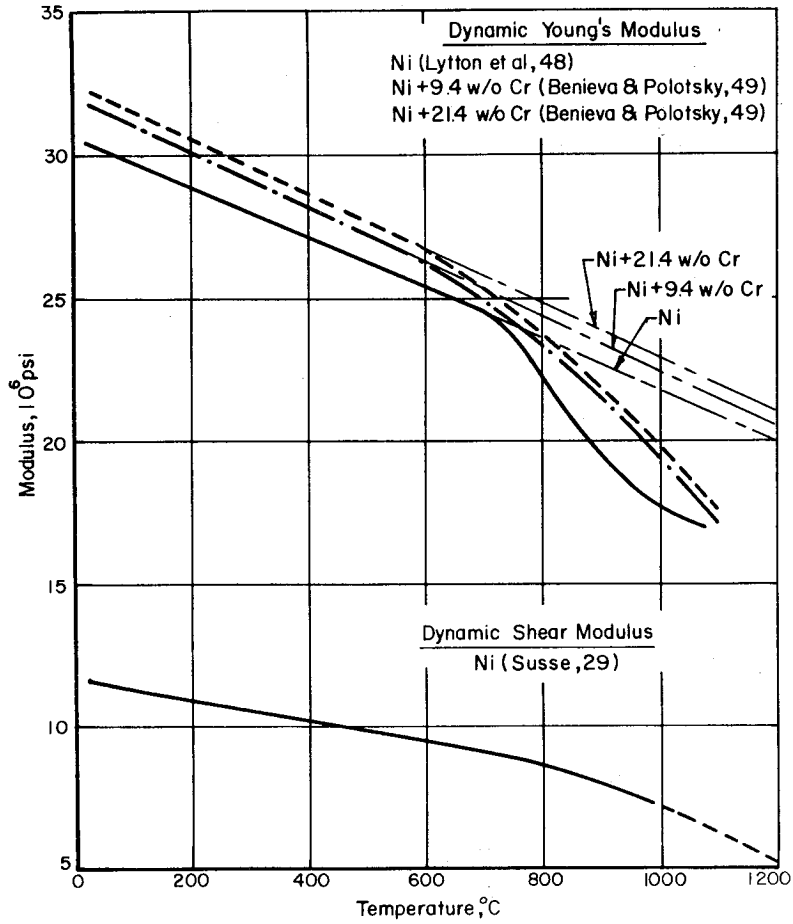
FIGURE A-1. TEMPERATURE DEPENDENCE OF DYNAMIC YOUNG'S AND SHEAR MODULI FOR Ni AND Ni-Cr ALLOYS
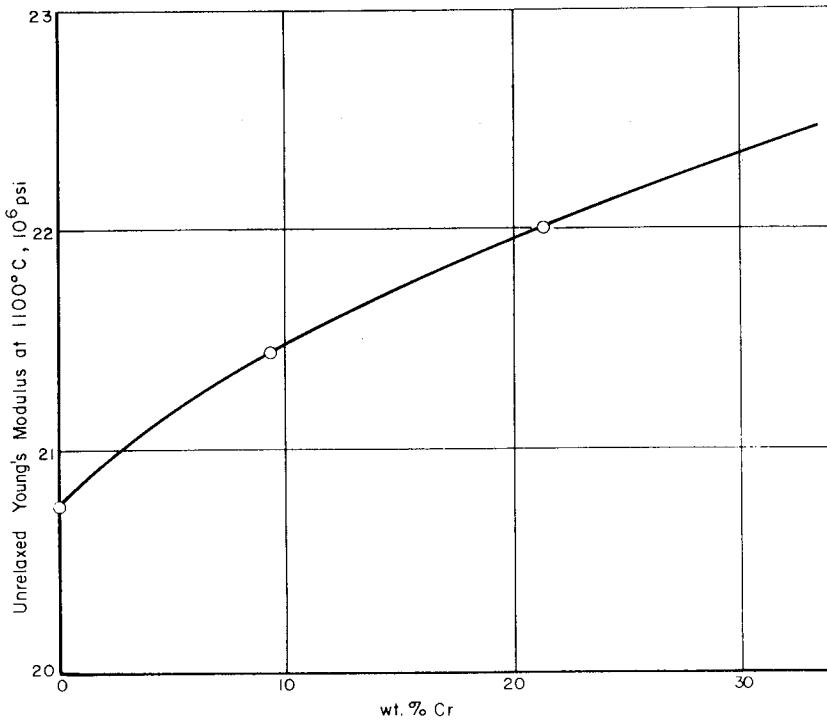
FIGURE A-2. UNRELAXED YOUNG'S MODULUS AT 1100°C AS A FUNCTION OF Cr CONTENT

Data are from extrapolations in Figure A-1.

extended dislocation nodes, and they calculated γ by the method due to Whelan[51]. The matrix stacking fault energies used in this work were determined from Figure A-3, and are: Ni-1ThO$_2$, γ = 240 erg/cm^2; Ni-13.5Cr-1ThO$_2$, γ = 140 erg/cm^2; Ni-22.6Cr-1ThO$_2$, γ = 80 erg/cm^2; and Ni-33.7Cr-1ThO$_2$, γ = 60 erg/cm^2. It is reasonable to assume that 1% of ThO$_2$ particles does not affect the matrix stacking fault energy.
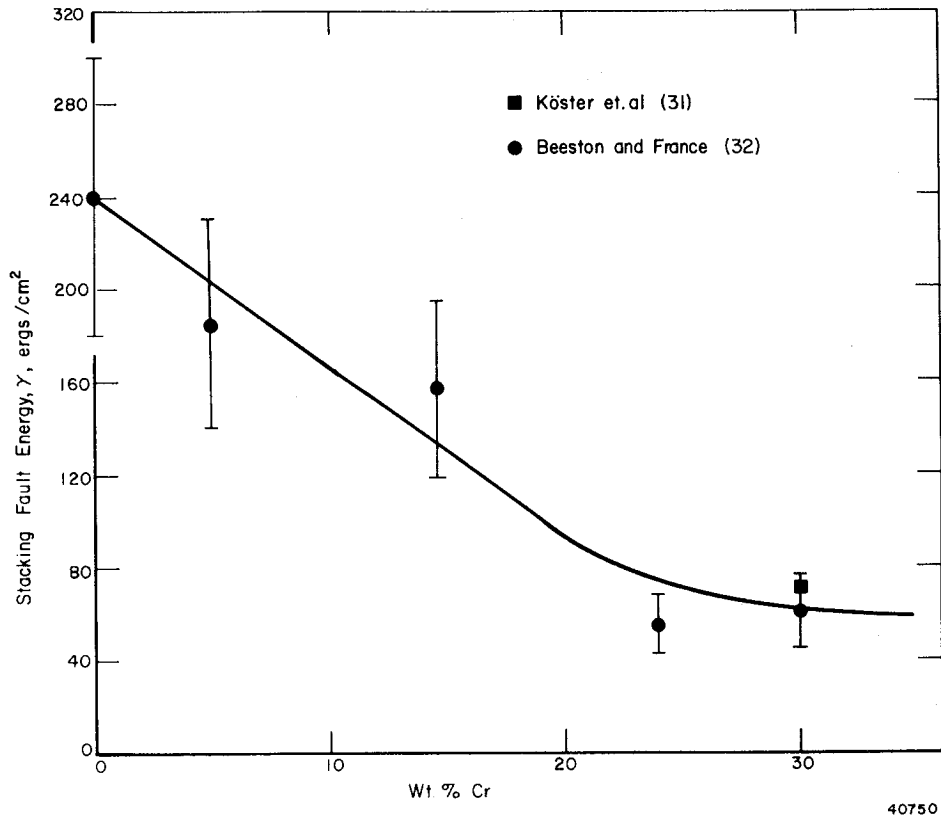
FIGURE A-3. THE EFFECT OF Cr ON THE STACKING
FAULT ENERGY OF Ni

DISTRIBUTION LIST FOR SUMMARY REPORT
CONTRACT NAS3-9413

ADDRESSEE		NUMBER OF COPIES	ADDRESSEE		NUMBER OF COPIES
NASA Headquarters			Aerospace Corporation		
Washington, D. C. 20546			P. O. Box 95085		
Attention: N. F. Rekos (RAP)		(1)	Los Angeles, California 90245		
R. H. Raring (RRM)		(1)	Attention: Dr. R. D. Carnahan		(1)
G. Deutsch (RRM)		(1)	Dr. K. Kamber		(1)
NASA-Lewis Research Center			Air Force Flight Dynamics Laboratory (FDTS)		
21000 Brookpark Road			Wright-Patterson AFB		
Cleveland, Ohio 44135			Dayton, Ohio 45433		
Attention: Technology Utilization Office	M.S. 3-19	(1)	Attention: SM Sgt. Jesse C. Ingram, Jr.		(1)
Report Control Office	M.S. 5-5	(1)			
Fluid System Components Division			AiResearch Manufacturing Company		
I. I. Pinkel	M.S. 5-3	(1)	9851-9951 Sepulveda Blvd.		
P. T. Hacker	M.S. 5-3	(1)	Los Angeles, California 90009		
			Attention: H. H. Block, Senior Metallurgist		(1)
Air-Breathing Engine Division					
J. Howard Childs	M.S. 60-4	(1)	American Society for Metals		
			Metals Park		
Air-Breathing Engine Procurement Section			Novelty, Ohio 44073		
John H. DeFord	M.S. 60-5	(1)	Attention: Dr. Taylor Lyman		(1)
Patent Counsel	M.S. 501-3	(1)	U. S. Army Materials Research Agency		
			Watertown Arsenal		
Materials & Stresses Division			Watertown, Massachusetts 02172		
S. S. Manson	M.S. 49-1	(1)	Attention: S. V. Arnold, Director		(1)
G. M. Ault	M.S. 105-1	(1)			
R. W. Hall	M.S. 49-1	(1)	Boeing Company		
J. W. Weeton	M.S. 49-1	(1)	Commercial Airplane Division		
J. Freche	M.S. 49-1	(1)	Materials Research Unit		
M. Quatinetz	M.S. 49-1	(1)	P. O. Box 707		
F. H. Harf	M.S. 105-1	(5)	Renton, Washington 98055		
A. Anglin	M.S. 105-1	(1)	Attention: Dr. D. Webster		(1)
N. T. Saunders	M.S. 105-1	(1)			
W. F. Brown, Jr.	M.S. 105-1	(1)	Boeing Company		
R. H. Kemp	M.S. 49-1	(1)	P. O. Box 733		
Dr. C. W. Andrews	M.S. 49-1	(1)	Renton, Washington 98055		
R. A. Signorelli	M.S. 106-1	(1)	Attention: Walter E. Binz, Jr.		
			SST Unit Chief		(1)
FAA Headquarters					
800 Independence Avenue S. W.			Curtiss-Wright Corporation		
Washington, D. C. 20553			Metals Processing Division		
Attention: F. B. Howard/SS-210		(1)	760 Northland Avenue		
Brig. Gen. J. C. Maxwell		(1)	Buffalo, New York 14215		
			Attention: B. Triffleman		(1)
Supersonic Transport Office					
Wright-Patterson AFB, Ohio 45433			McDonnell Douglas Corporation		
Attention: SESHS, J. L. Wilkins		(2)	Materials Research Division		
			3000 Ocean Park Blvd.		
NASA Scientific & Technical Information Facility			Santa Monica, California 90406		
P. O. Box 3300			Attention: Dr. D. Killpatrick		(1)
College Park, Maryland 20740					
Attention: NASA Representative RQT-2448		(6)			

DISTRIBUTION LIST
(Continued)

ADDRESSEE	NUMBER OF COPIES	ADDRESSEE	NUMBER OF COPIES
Defense Documentation Center (DDC) Cameron Station 5010 Duke Street Alexandria, Virginia 22314	(1)	NASA-Ames Research Center Moffet Field, California 94035 Attention: Library	(1)
AFML Wright-Patterson AFB, Ohio 45433 Attention: N. Geyer (MAMP)	(1)	NASA-Goddard Space Flight Center Greenbelt, Maryland 20771 Attention: Library	(1)
Dr. A. M. Lovelace, Director (MAG)	(1)	NASA-Flight Research Center P. O. Box 273 Edwards, California 93523 Attention: Library	(1)
E. Beardslee (MAAE)	(1)		
R. O. Hughes (MAAM)	(1)		
C. Lombard (MAMP)	(1)		
Dr. H. M. Burte (MAM)	(1)	Department of the Navy U. S. Navy Marine Engineering Lab. Annapolis, Maryland 21402 Attention: Dr. Klaus M. Zwilsky	(1)
T. D. Cooper (Materials & Ceramics)	(1)		
Department of the Navy ONR Code 429 Washington, D. C. 20350 Attention: Dr. R. Roberts	(1)	Air Reduction Company Central Research Lab. Murray Hill, New Jersey 07971 Attention: Dr. E. Gregory	(1)
Chief, Bureau of Naval Weapons Department of the Navy Washington, D. C. 20350 Attention: RRMA-2/T. F. Kearns	(1)	Lockheed Missile and Space Company Palo Alto, California 94304 Attention: Dr. E. C. Burke, Materials Science Lab.	(1)
NASA-Langley Research Center Langley Station Hampton, Virginia 23365 Attention: Technical Library	(1)	Dr. T. E. Tietz, Materials Science Lab.	(1)
E. E. Mathauser	(1)	R. M. Bonesteel, Materials Science Lab.	(1)
Irvin Miller MS 214	(1)		
NASA-Manned Spacecraft Center Structures & Mechanics Division 2101 Webster-Seabrook Road Houston, Texas 77058 Attention: Branch Chief (ES441)	(1)	Lockheed Palo Alto Research Labs. Materials & Science Lab 52-30 3251 Hanover Street Palo Alto, California 94304 Attention: Dr. Clause G. Goetzel	(1)
Library	(1)		
U. S. Army Aviation Materials Lab. Fort Eustis, Virginia 23604 Attention: John White, Chief, SMOFE-APG	(1)	Lockheed-Georgia Company Research Laboratory Marietta, Georgia 30060 Attention: Dr. W. S. Cremens	(1)
Jet Propulsion Laboratory 4800 Oak Grove Drive Pasadena, California 91103 Attention: Library	(1)	Department of Metallurgy University of British Columbia Vancouver, B. C., Canada Attention: Prof. D. Tromans	(1)
		Titanium Metals Corp. of America 233 Broadway New York, New York 10007 Attention: Ward Minkler, Mgr. of Technical Service	(1)

ADDRESSEE	NUMBER OF COPIES	ADDRESSEE	NUMBER OF COPIES
Ford Motor Company Ford Scientific Lab 20,000 Rotunda Drive Dearborn, Michigan 48124		The Ohio State University Columbus, Ohio 43210 Attention: Prof. M. G. Fontana Prof. J. P. Hirth	(1) (1)
Attention: Dr. T. L. Johnston Dr. C. Laird	(1) (1)	Pratt & Whitney Aircraft Division United Aircraft Corporation 400 Main Street East Hartford, Connecticut 06108	
General Electric Company Materials & Process Laboratories Schenectady, New York 12301 Attention: C. T. Sims	(1)	Attention: E. F. Bradley G. Andreini F. Talboom Research Division Library	(1) (1) (1) (1)
General Electric Company Advanced Technology Lab Schenectady, New York 12305	(1)	Solar, A Division of International Harvester 2200 Pacific Highway San Diego, California 92112	
General Electric Company Materials Devel. Lab. Oper. Advanced Engine & Technology Dept. Cincinnati, Ohio 45215		Attention: J. V. Long	(1)
Attention: L. P. Jahnke W. Chang	(1) (1)	Sylvania Electric Products, Inc. Chemical & Metallurgical Division Towanda, Pennsylvania 18848 Attention: Dr. J. S. Smith	(1)
International Nickel Company Paul D. Merica Research Laboratory Sterling Forest Suffern, New York 10901		TRW Inc. TRW Electromechanical Division 23,555 Euclid Avenue Cleveland, Ohio 44117	
Attention: Dr. F. Decker Dr. H. Merrick	(1) (1)	Attention: Dr. G. Doble Dr. R. Quigg	(1)
International Nickel Company 67 Wall Street New York, New York 10005 Attention: R. R. Dewitt	(1)	Universal-Cyclops Steel Corporation Bridgeville, Pennsylvania 15017 Attention: C. P. Mueller	(1)
International Nickel Company Huntington, W. Virginia 25701 Attention: Library	(1)	University of California at Los Angeles Los Angeles, California 90024 Attention: Dr. G. Hoffman	(1)
Massachusetts Institute of Technology Department of Metallurgy Rm. 8-305 77 Massachusetts Avenue Cambridge, Massachusetts 02138		Vitro Laboratories 200 Pleasant Valley Way West Orange, New Jersey 07052	
Attention: Prof. N. J. Grant	(1)	Attention: Dr. S. Grand	(1)
Narmco Research & Development Division Whittaker Corporation 3540 Aero Court San Diego, California 92123		U. S. Atomic Energy Commission Washington, D. C. 20545 Attention: Jules Simmons Technical Reports Library Dr. W. F. Sheely	(1) (1) (1)
Attention: Dr. F. J. Riel, Technical Director	(1)	Air Force Office of Scientific Research 1400 Wilson Blvd. Arlington, Virginia 22209 Attention: SREP	(1)

ADDRESSEE	NUMBER OF COPIES	ADDRESSEE	NUMBER OF COPIES
Gordon McKay Laboratory Harvard University Cambridge, Massachusetts 02138 Attention: Dr. M. F. Ashby	(1)	Defense Metals Information Center (DMIC) Battelle Memorial Institute 505 King Avenue Columbus, Ohio 43201	(1)
Advanced Materials Research & Development Lab. Pratt & Whitney Aircraft Middletown, Connecticut 06473 Attention: Dr. D. H. Boone	(1)	E. I. DuPont de Nemours & Co. Metal Products Sales Wilmington, Delaware 19898 Attention: Dr. W. I. Pollock	(1)
Solid State Sciences Div. The Franklin Institute Philadelphia, Pennsylvania 19103 Attention: Dr. B. Banerjee	(1)	General Motors Corporation Allison Division Indianapolis, Indiana 46206 Attention: D. K. Hanink, Materials Lab.	(1)
University of California Hearst Mining Bldg. - Room 268 Berkeley, California 94720 Attention: Prof. J. E. Dorn	(1)	Ilikon Corporation Natick Industrial Center Natick, Massachusetts 01762 Attention: Dr. L. J. Bonis	(1)
Materials Division Central Electricity Research Laboratory Kingston Road Leatherhead, Surrey England Attention: Dr. R. K. Ham	(1)	Arthur D. Little, Inc. 20 Acorn Park Cambridge, Massachusetts 02140 Attention: Dr. B. Bovarnick	(1)
Dept. of Materials Science Pennsylvania State University University Park, Pennsylvania 16802 Attention: Prof. M. C. Inman	(1)	National Research Corporation 70 Memorial Drive Cambridge, Massachusetts 02142 Attention: Technical Information Center	(1)
Central Electricity Generating Board Berkeley Nuclear Lab. Berkeley, Gloucestershire England Attention: Dr. R. B. Jones	(1)	Teledyne Materials Research Company 303 Bear Hill Road Waltham, Massachusetts 02154 Attention: Dr. R. Widmer	(1)
Department of Materials Science Stanford University Stanford, California 94305 Attention: Prof. O. D. Sherby Prof. C. Barrett	(1) (1)	Rensselaer Poly Tech. Troy, New York 12180 Attention: Prof. Fritz V. Lenel Prof. George S. Ansell	(1) (1)
Department of Metallurgy Pembroke Street Cambridge University Cambridge, England Attention: G. C. Smith	(1)	Sherritt Gordon Mines, Ltd. Research & Development Division Fort Saskatchewan Alberta, Canada Attention: Dr. R. W. Fraser Dr. D.J.I. Evans Dr. F. L. Norris	(1) (1) (1)
		Northwestern University Department of Metallurgy Evanston, Illinois 60201 Attention: Prof. J. Weertman	(1)

ADDRESSEE	NUMBER OF COPIES
Case Western Reserve University University Circle Cleveland, Ohio 44106 Attention: Prof. L. Leonard, Dept. of Metallurgy	(1)
Dept. of Physical Metallurgy University of Birmingham Edgebaston Birmingham, England Attention: Prof. R. E. Smallman	(1)
Dept. of Metallurgy University of Kentucky Lexington, Kentucky 40506 Attention: Prof. Hans Conrad	(1)
National Physical Laboratory Teddington, Middlesex England Attention: Dr. D. McLean	(1)
Battelle-Institut e. V. Wiesbadenstrasse, Postfach 1337 Frankfurt/Main, W. 13 Germany Attention: R. Scharwaechter	(1)
Atomic Energy of Canada Ltd. CRNL Applied Materials Research Branch Chalk River, Ontario, Canada Attention: Dr. C. D. Williams	(1)
Westinghouse Astronuclear Lab. Metallurgy Department P. O. Box 10864 Pittsburgh, Pennsylvania 15236 Attention: R. T. Begley	(1)